6.2.5 HIL-Measurement Results

The following subsections of the HIL-measurement results correspond to the different channel configurations in the test case description of Sec. 6.2.1.2.

6.2.5.1 HIL-Measurements using Measured LTE Channels in Channel Emulator

In this HIL test, OFDM signals with 2048 subcarriers and CP length of 144 samples were transmitted, which comply with the LTE standard. The transmission signal bandwidth was 20 MHz. Moreover, the measured LTE channels reported in [23] were used (i.e. loaded in the channel emulator). The scenario (setup) of the channel measurement is shown in Fig. 6.29, where the UTs are static. Thus, the channels are also static. The distance between the two UTs were 25 meter. Moreover, both UTs are about 485 meters away from the BS. This scenario of the channel measurement is very typical for the considered full sharing scenario. In the HIL measurement, the "triggering" mode of the channel emulator was used.

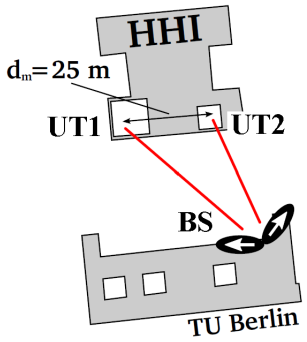

Figure 6.29: The setup for the measurement of the LTE channels used for the full sharing scenario.

Fig. 6.30 shows the estimated channel frequency response of the LTE channels including the influence of the RF chains. The transmission bandwidth is 20 MHz, at the carrier frequency of 2.4 GHz. For all precoding schemes, we use a per-subcarrier power constraint. Different SNRs are achieved at the UTs by adjusting the Tx power.

Fig. 6.31 shows the measured sum rates (capacity) of the different precoding schemes as well as of the non-sharing case as functions of SNR. The per operator rate (capacity) is also shown in Fig. 6.32. As shown, both sum rate gain and per-user rate gain can be achieved by sharing the spectrum. The higher the SNR, the larger the sharing gain. Furthermore, RBD generally outperforms BD. In the low SNR range, the sum rate of BD can be even lower than the case without spectrum sharing. In contrast, with RBD, sum rate gain can be achieved over the whole observed SNR

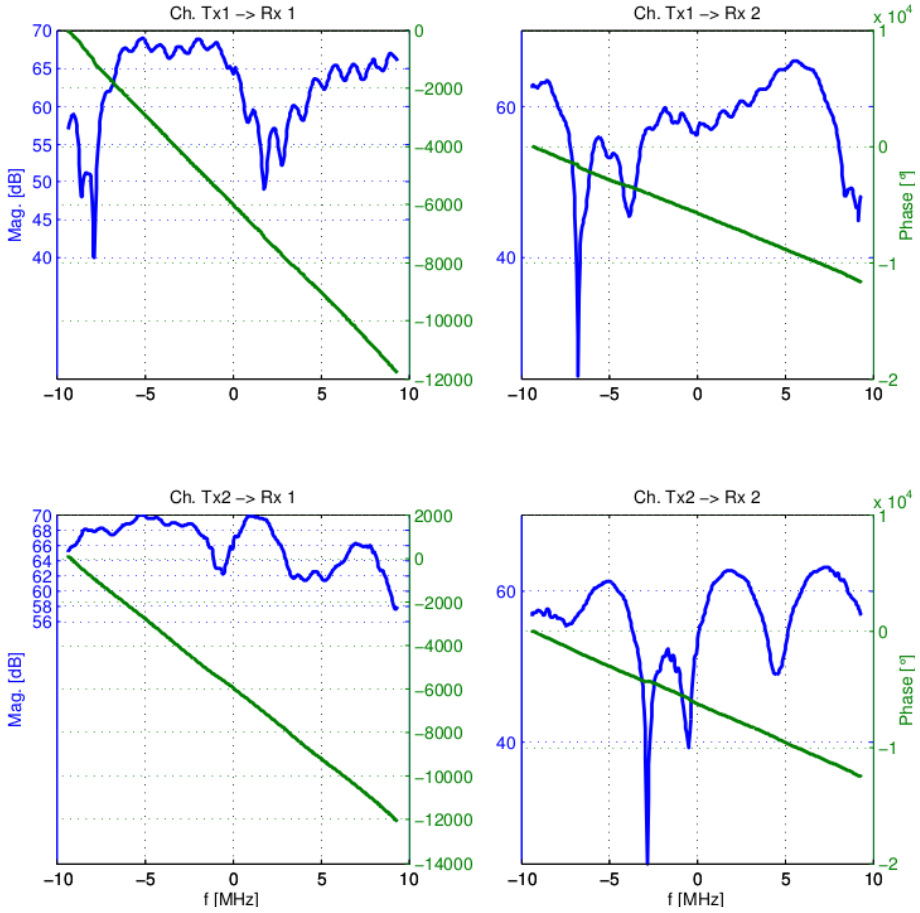

Figure 6.30: Frequency response of the measured LTE channels.

range. However, we should keep in mind that RBD require both CSI and noise power information at the BS, while BD only requires CSI at the BS. Therefore, RBD requires more feedback overhead, and there exists a tradeoff between performance and overhead among these two precoding algorithms. Finally, compared to the spectrum sharing scenario SC2-TA (i.e. the results in Fig. 6.11), the spectrum sharing gain in the full sharing scenario is comparably smaller. The reason is that in the spectrum sharing scenario, the signals are transmitted from two separate BS's with individual power controlls. By using per-subcarrier power constraint, the total transmit power (over both BS's) in the spectrum sharing case is about a double of the case of non-sharing. In contrast, in this full sharing scenario, only one BS is transmitting, both in sharing and non-sharing cases. No matter whether the spectrum is shared, the BS is transmitting over the whole available spectrum. Furthermore, the per-subcarrier power constraint in the spectrum sharing case will be a constraint over the multiplexed signal of both operators. Therefore, the total transmit power of the spectrum sharing case is approximately the same as that of the non-sharing case, leading to a reduced spectrum sharing gain compared to the scenario SC2-TA.

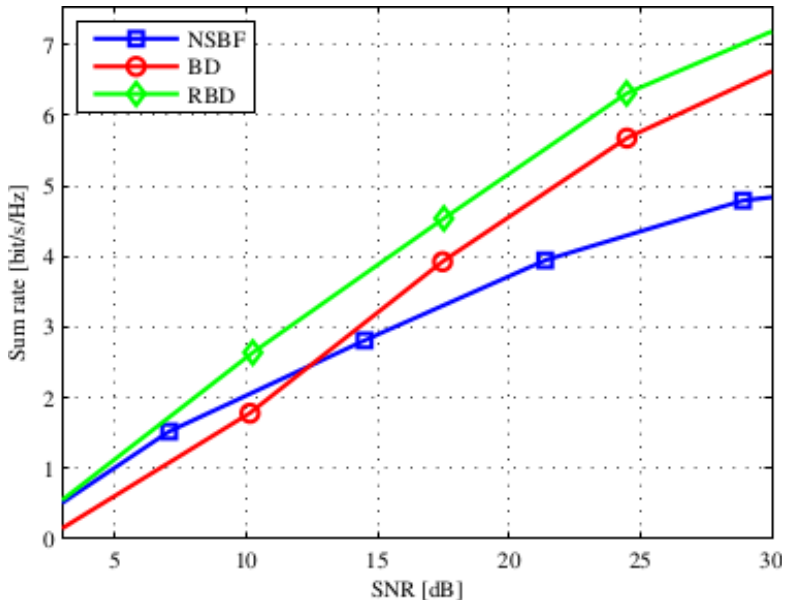

Figure 6.31: Measured sum rate vs. SNR. NSBF: non-sharing case with MRT.

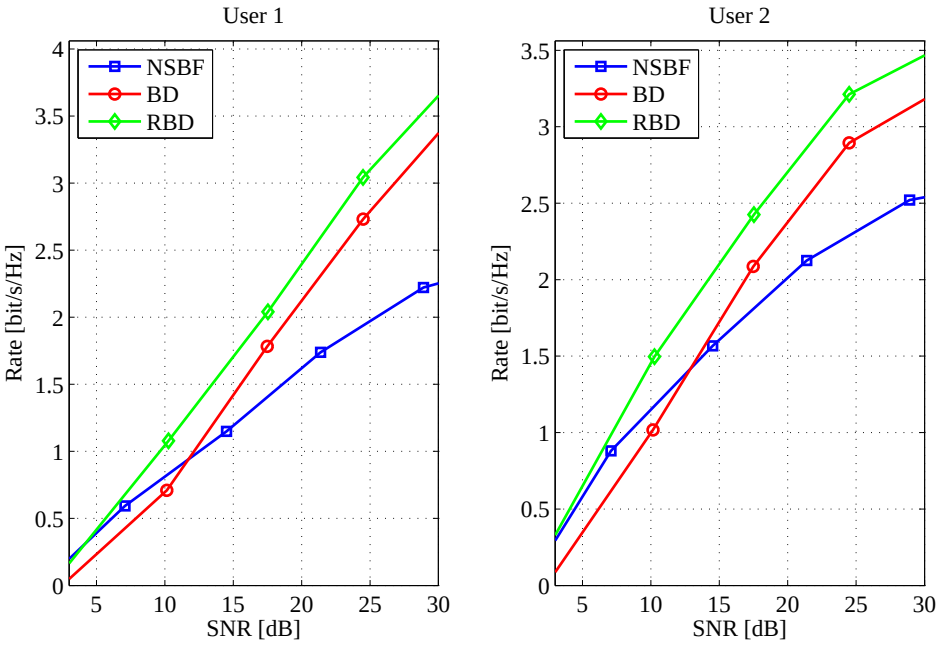

Figure 6.32: Measured per user rate vs. SNR. NSBF: non-sharing case with MRT.

6.2.5.2 HIL-Measurements using 60 GHz Free-Space Transmission

In the HIL test with the 60 GHz transmission mode, OFDM signals with 256 sub-carriers and CP length of 32 samples were transmitted. These numbers were chosen according to the propagation characteristics of the indoor 60 GHz channel and the

transmission bandwidth, which is 80 MHz. Fig. 6.33 shows an example of the measured frequency response of the measured 60 GHz channels with Tx-Rx distance of about 2 meters.

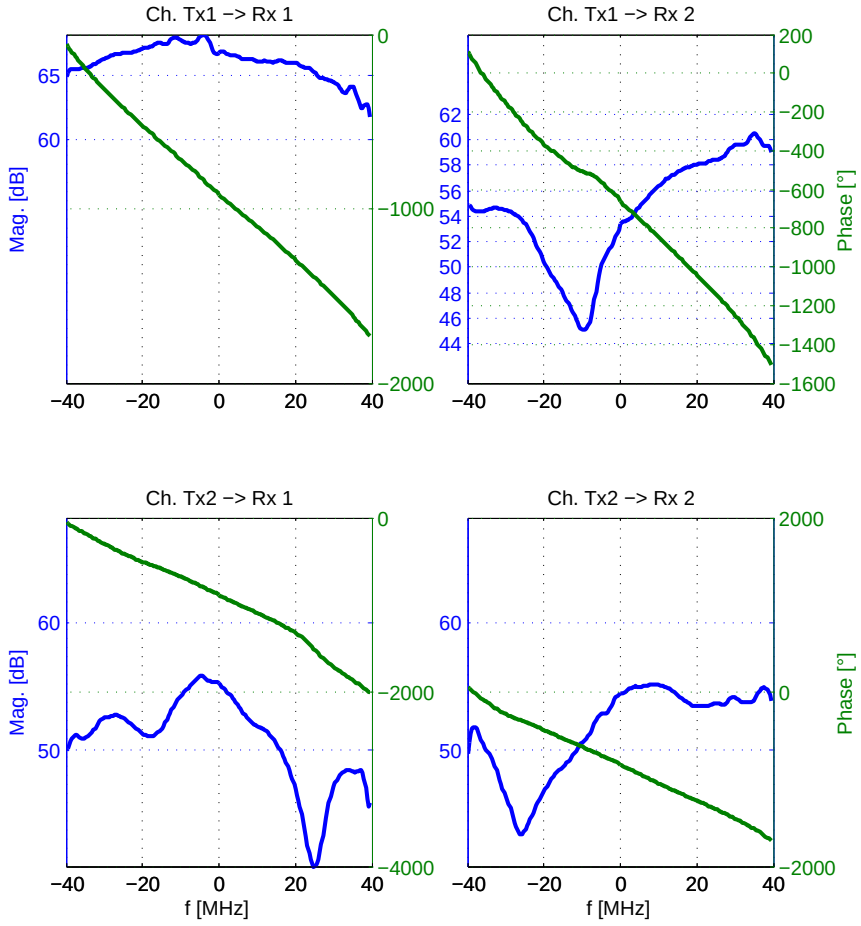

Figure 6.33: Frequency response of the measured 60 GHz channels.

Fig. 6.34 shows the measured received signal constellation (with QPSK) in the sharing case with BD- and RBD precoding algorithm as well as in the non-sharing case with EMBF. Both the cases with and without additional Rx equalization are shown. As can be seen, slight amplitude and phase distortions of the constellations are present, which were probably caused by channel variation or time synchronization error). We can see that these distortions can be corrected by the additional Rx equalization. Interestingly, the noise and interference level of constellations in the sharing cases and the non-sharing case are almost the same. Fig. 6.35 shows the CCDF of the instantaneous sum rates of each scheme. From this figure, we can also also see the gain due to spectrum sharing and the benefit of the additional Rx equalization.

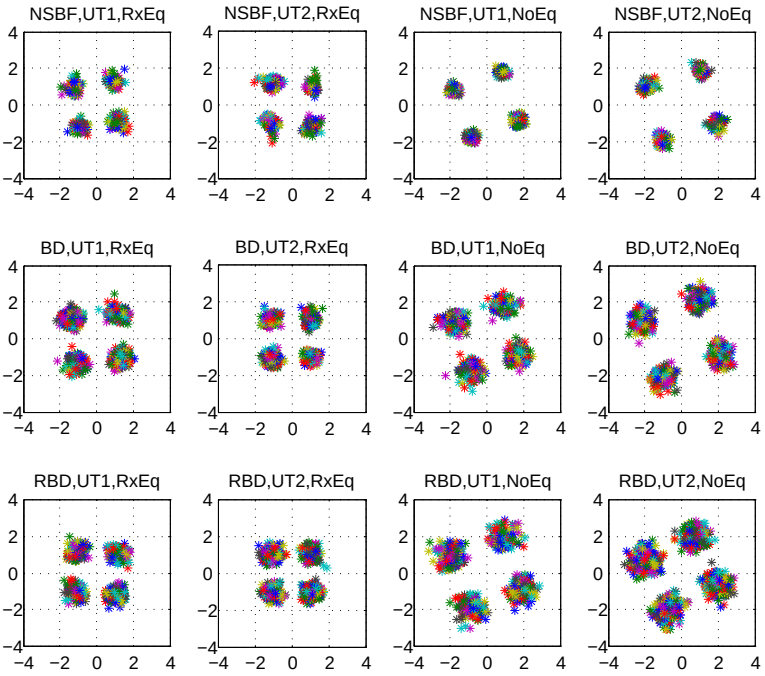

Figure 6.34: Measured received signal constellation in the sharing and non-sharing cases. Both cases with and without Rx equalization are shown.

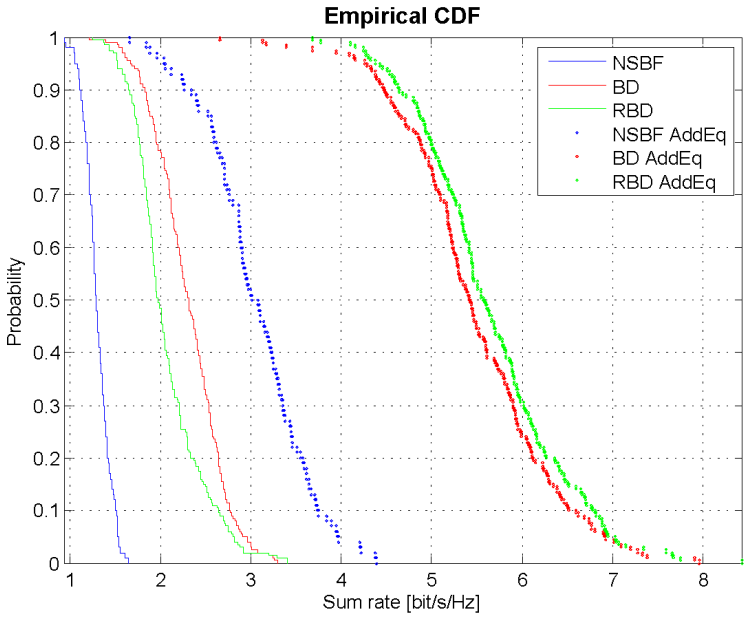

Figure 6.35: CCDF of the instantaneous sum rate in the sharing and non-sharing cases. Both cases with and without Rx equalization are shown.

Fig. 6.36 shows the instantaneous measured sum throughput of the different cases. As shown, the sharing cases have much higher throughput than the non-sharing case. Note that the throughput is limited to the use of QPSK modulation, while the sum rate mentioned above is not limited to the used modulation but calculated directly from the Shannon equation. Furthermore, the gain by additional equalization is not obvious here. The reason is that by using QPSK, the above mentioned amplitude and phase distortions have negligible influence on the throughput. However, if higher modulation is used, the gain of the additional equalization will be more obvious.

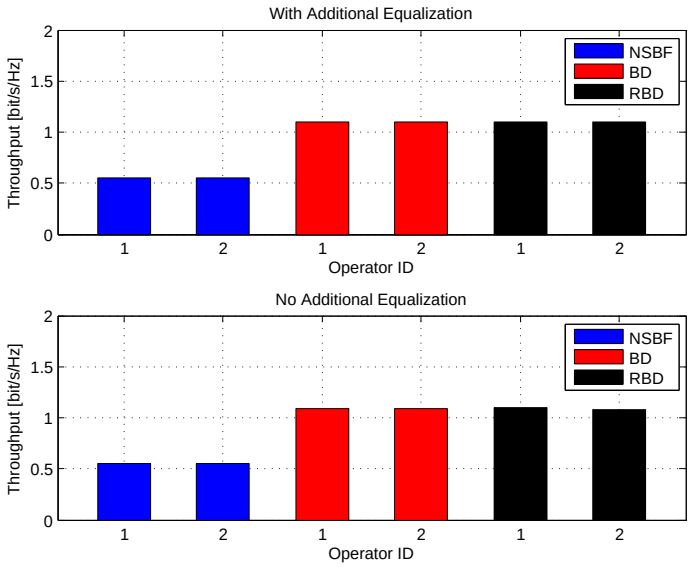

Figure 6.36: Measured sum throughput of the different schemes using QPSK. Both the cases with and without additional Rx equalization are shown.

6.3 Scenario SC1-TC-I: Relay Sharing in "Butterfly" Network

6.3.1 Scenario and Test Case Description

6.3.1.1 Scenario Description

As shown in Figure 6.37, this scenario consists of a "butterfly" network topology, where two independent data sources, SA and SB, of different operators should transmit data to the destinations DA and DB, respectively, via two-phase relaying transmission. Both relay station and spectrum are shared between operators. In

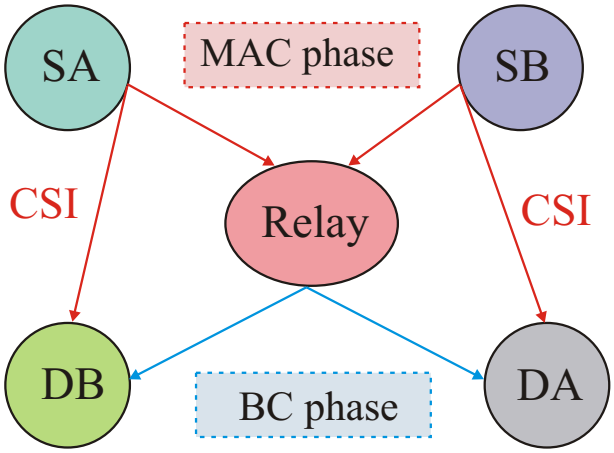

Figure 6.37: Abstracted model of Scenario SC1-TC-I.

the Multiple Access (MAC[8]) phase, SA and SB transmit data to the relay and to the destinations DB and DA, respectively. Note that there is no direct link between a source and its dedicated destination. The received data of DA and DB in the MAC phase are called Complementary-Side-Information (C-SI, [6]). In the BroadCast (BC) phase, the relay transmits data to both destinations. The destinations decode the dedicated data based on the data from the relay and the C-SI. Since both relay and spectrum are shared, the data streams of SA and SB will be superimposed at the relay and cause interference to each other. To suppress such interference and achieve maximum capacity, sophisticated relaying strategy should be applied. While Figure 6.37 provides an abstracted illustration of this scenario, Fig. 6.38 and Fig. 6.39 show how this scenario correspond to practical mobile networks. As shown, the two data sources can be either BS's or UT's of two different operators. The direct link for the desired communication pairs are blocked by high buildings. Therefore, a relay station can be put on on of such high buildings to asist the desired communication. Meanwhile, the transmitters and receivers of different operators can have direct links or even close to each other, although they are not within a desired communication pair. However, the communication between such transmitters and receivers can generate C-SI, which helps the desired communication via the relay.

6.3.1.2 Test Case Description

As PHY-layer technique, OFDM with BPSK modulation and LDPC coding of code rate $\frac{1}{2}$ is applied. The OFDM parameters are similar to those in scenario SC2-TA (Ch. 6.1). Since no LTE measurements have been done for this scenario, Rayleigh

[8]Only within Ch. 6.3 and Ch. 6.4, the abbreviation "MAC" is used to indicate "Multiple Access".

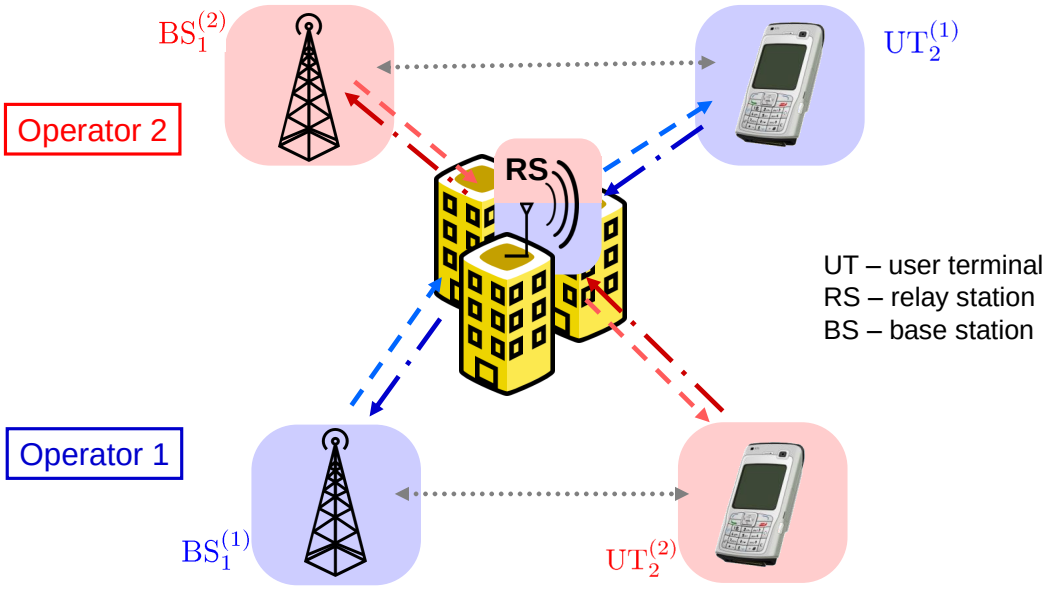

Figure 6.38: Scenario SC1-TC-I: Relay and spectrum sharing. Communication between BS's and UT's.

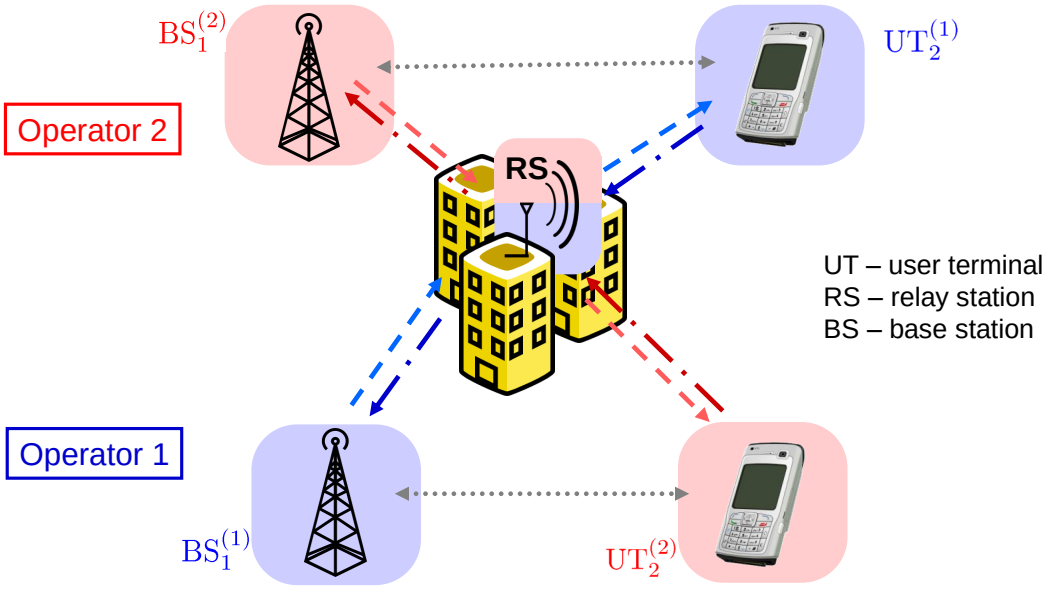

Figure 6.39: Scenario SC1-TC-I: Relay and spectrum sharing. Communication directly between UT's (Terminal to terminal communication).

channels are used. Moreover, single antenna transmission and global time synchronization are assumed.

In the HIL test of this scenario, we assume the sharing of the relay station (as infrastructure). Under this assumption, we perform the following comparisons and investigations:

- To verify the spectrum sharing gain, the case without spectrum sharing should be compared with the case with spectrum sharing. In the case without spectrum sharing, the two sources use orthogonal frequency bands. Thus, without spectrum sharing, no interference is present between operators and the relay applies normal Decode-and-Forward (DF) strategy. In this case, orthogonal frequency bands are used, the available frequency band for each operator is only the half of those in the spectrum sharing cases.
- In the case of spectrum sharing, different possible relaying techniques should be compared, which enable spectrum sharing. After such comparison, the suitable technique can be identified for the practical deployment.

Two performance criteria are applied. The first one is the sum rate of the whole network in bits/s/Hz, which is mainly evaluated for coded transmissions. For the calculation of the sum rate, the CP and NULL-subcarrier overhead of the OFDM system as well as the transmission overhead of the two-phase-relaying are considered. The second one is the sum capacity in bits/symbol, which is evaluated both for uncoded and coded transmissions. Both criteria will be evaluated for different Rx SNR values as well as different SNR values in the C-SI links. For simplicity, we assume that the Rx SNR (at the relay) in the MAC-phase is always equal to the Rx SNR in the BC-phase (at the destinations). Moreover, all C-SI links should have the same SNR value.

6.3.2 Enabling Algorithms

Two relaying strategies are applied for interference suppression and capacity maximization: Hierarchical Decode and Forward (HDF, [6]) and Amplify-and-Forward with Successive Interference Cancellation (AF-SIC, [30]). The HDF strategy is developed within SAPHYRE project, while AF-SIC is a conventional strategy. For the OFDM system under investigation, both techniques are applied subcarrier-wise. These two strategies are briefly described as follows, assuming frequency-flat channels (which is the equivalent case within each OFDM subcarrier):

6.3.2.1 Hierarchical Decode and Forward (HDF)

We assume the coder $\mathcal{C}$ to be a LDPC coder and $\mathcal{M}$ the BPSK mapper. Also $\mathcal{M}^{-1}$ to be the soft output BPSK demodulator based on the minimal Euclidean distance and $\mathcal{C}^{-1}$ to be the LDPC decoder. There are assumed i.i.d. data vectors

$\boldsymbol{d}_A$ and $\boldsymbol{d}_B$ inputing the LDPC coders $\mathcal{C}$. The output codewords $\boldsymbol{c}_A = C(\boldsymbol{d}_A)$ and $\boldsymbol{c}_B = C(\boldsymbol{d}_B)$ then input the BPSK signal space mapper $\mathcal{M}$ to form the output signal space vectors $\boldsymbol{s}_A = \mathcal{M}(\boldsymbol{c}_A)$ and $\boldsymbol{s}_B = \mathcal{M}(\boldsymbol{c}_B)$. The signal inputing the relay R is $\boldsymbol{x}_R = \boldsymbol{s}_A h_{AR} + \boldsymbol{s}_B h_{BR} + \boldsymbol{w}_{MAC}$, while the signal inputing the destination D_A is $\boldsymbol{y}_A^{MAC} = \boldsymbol{s}_B + \boldsymbol{w}_{BA}$. Moreover, the signal inputing the destination D_B is $\boldsymbol{y}_B^{MAC} = \boldsymbol{s}_A + \boldsymbol{w}_{AB}$. Within the relay, the minimal Euclidean metric

$$\mu_{AB}^k = \min_{i,j:k=\mathcal{X}(i,j)} |x_R - s_A^i h_{AR} - s_B^j h_{BR}|^2$$

is evaluated in the relay (outer code caring about the exclusivity). Then the hierarchical data are decoded by $\hat{\boldsymbol{d}}_{AB} = \mathcal{C}^{-1}(\boldsymbol{\mu}_{AB})$ (inner code caring about the coding gain). The signal space vector inputing the BC-phase is given by $\boldsymbol{s}_R = \mathcal{M}(\mathcal{C}(\hat{\boldsymbol{d}}_{AB}))$. In the BC phase, the signal inputing the destination D_A is $\mathbf{y}_A^{BC} = \boldsymbol{s_R} + \boldsymbol{w}_{BC}$, whereas the signal inputing the destination D_B is $\mathbf{y}_B^{BC} = \boldsymbol{s_R} + \boldsymbol{w_{BC}}$. At the destination, the following C-SI's are used: $\boldsymbol{d}_A^{C-SI} = \mathcal{C}^{-1}(\mathcal{M}^{-1}(\boldsymbol{y}_B^{MAC}))$ and $\boldsymbol{d}_B^{C-SI} = \mathcal{C}^{-1}(\mathcal{M}^{-1}(\boldsymbol{y}_A^{MAC}))$. First, the relay-decoded hierarchical data $\hat{\hat{\boldsymbol{d}}}_{AB} = \mathcal{C}^{-1}(\mathcal{M}^{-1}(\mathbf{y}_A^{BC})$ is decoded. Finally, by exploiting the C-SI $\boldsymbol{d}_B^{C-SI}$, the data vector is decoded as: $\hat{\boldsymbol{d}}_A = \hat{\hat{\boldsymbol{d}}}_{AB} \oplus \boldsymbol{d}_B^{C-SI}$, where $\oplus$ denotes bit-wise XOR operation.

6.3.2.2 Amplify-and-Forward with Successive Interference Cancellation (AF-SIC)

The main signal transmission process of with AF-SIC is generally the same as with HDF. The main differences are the relay processing and the destination processing. With AF-SIC strategy, the relay transmits $\boldsymbol{s}_R = \boldsymbol{x}_R \beta$, where $\beta = 1/\sqrt{h_{AR}^2 + h_{BR}^2 + N_0}$ (see [30]). At the destination A, the signal is reconstructed from the C-SI as follows: $\boldsymbol{s}_A^{C-SI} = (\boldsymbol{y}_A^{BC} - h_{BR}\mathcal{M}(\mathcal{C}(\boldsymbol{d}_B^{C-SI})))/h_{AR}$ and the data $\hat{\boldsymbol{d}}_A = \mathcal{C}^{-1}(\mathcal{M}^{-1}(\boldsymbol{s}_A^{C-SI})$. The reconstruction of $\hat{\boldsymbol{d}}_B$ follows a similar way. Note that the two way relaying in [30] can be regarded as the special case that SA=DB and SB=DA, which implies perfect C-SI. Thus, the 2-step scheme in [30] can be easily extended to "butterfly" network.

6.3.3 Practical Implementation Issues

In this scenario, no BF- or precoding techniques are applied. Therefore, the practical implementation problems mentioned in Sec. 6.1.3 are relaxed. But still, several practical implementation aspects have to be considered. First, since the channel estimation and the corresponding signal equalization are carried out within the same signal frame, these two procedures are consistent. Furthermore, since no CSI is required at the transmitters, no CSI feedback scheme is necessary. This is a very favorable character of the proposed techniques. Second, time synchronization error that is within the tolerable range of CP just changes the effective channel, which will be corrected by the channel equalization. Moreover, rate estimation is not

necessary. However, frequency synchronization is necessary, since the proposed algorithm concerns a single subcarrier (frequency). Frequency synchronization error will cause model mismatch and degrade the performance. Furthermore, the signal amplitude scaling for DACs and the rescaling of the channel coefficients are necessary. Therefore, both sources may have to exchange such scaling information or just use a fixed scaling factor. Finally, the effect of colored noise should also be considered.

Actually, regarding the synchronization of the source nodes, the following two cases have to be considered:

1. The source nodes are BSs: In this case, all BSs of the involved operators should be synchronized accurately using time and frequency reference signals from GPS or the backbone network [31];
2. The source nodes are UTs: In this case, all involved UTs should first estimate their CFO and pre-compensate it before transmission. The estimation of these CFOs can be done based on a broadcasted training sequence (during connection establishment) by the relay. The time synchronization can be coordinated by the relay in a similar way as the BSs (via standard procedures).

Furthermore, the assumption of no direct link between each source and its dedicated sink may not be realistic. In the reality, there could still be weak links between each source and its dedicated sink, which is not sufficient for data detection but can disturb the reception of the C-SI. Thus, slightly corrupted C-SI links must be taken into account. In our HIL test, we have tested the cases with C-SI of different SNR levels, which can more or less equivalent model the disturbance from the direct links. It will be shown that the proposed algorithms can work well even in the case of bad C-SI quality.

6.3.4 Mapping on the HIL-Demonstrator Platform

For the HIL test of this scenario, the mapping was done with two modes: 1) The RF cable network mode assisted with multi-stage mapping technique; 2) The channel emulator mode. For simplicity in the RF cable network mode, only one physical transmitter and one physical receiver (from different experimental devices) were used. With multi-stage mapping, the desired scenario with three transmitters (SA, SB, relay) and three receivers (DA, DB, relay) can be mapped. Furthermore, Rayleigh channels effects are generated in MATLAB before the signal transmission in hardware. The advantage of this mapping is that the SNR of the direct links and the C-SI links can be easily adjusted by adding artificial noise to obtain performance evaluation on a two dimensional plane of these SNR's. The mapping using channel emulator mode is illustrated in Fig. 6.40. In this mapping mode, 3 transmitter and 3 receivers are selected from the two experimental devices. Two transmitters play the roles of SA and SB, while the third one plays the role of the shared relay. Two

receivers play the roles of DA and DB, while the third one also plays the role of the shared relay. The corresponding Rayleigh channels are generated in the channel emulator.

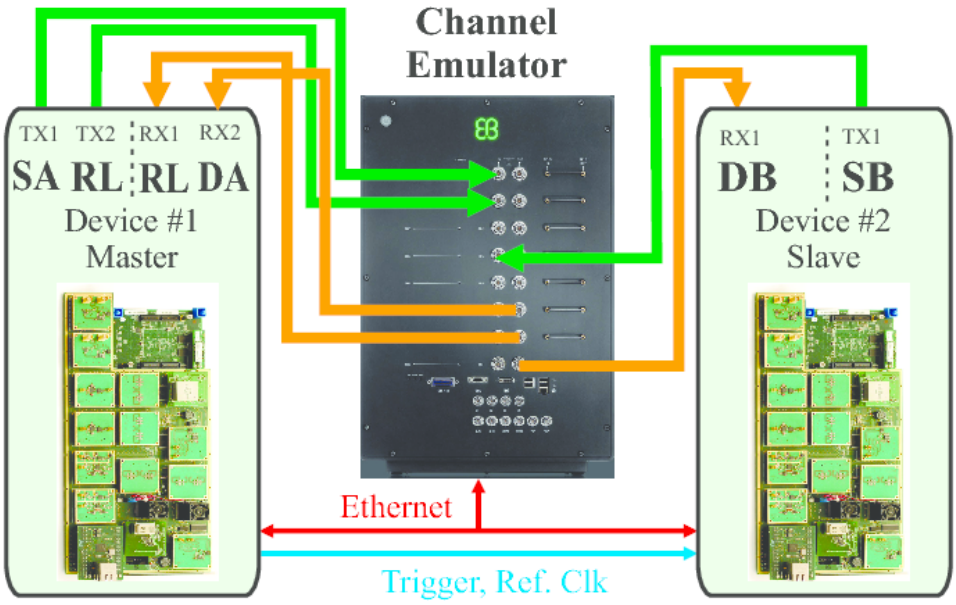

Figure 6.40: Mapping of scenario SC1-TC-I on the HIL platform with the channel emulator mode.

Fig. 6.41 shows the flowchart of the HIL test program. First, general parameter settings are carried out. Afterwards, the channel set up is carried out including the selection of the channel mode and the loading of the channel files. Afterwards, channel realization control and channel estimation are carried out. With each channel realization, different SNR levels are applied by adding artificial noise or by adjusting the variable gain amplifiers at the modulators. For each channel realization and each SNR level, signal transmissions in the H-MAC and the H-BC phases with both non-spectrum sharing and spectrum sharing are carried out one after another. In the sharing case, different relay algorithms are applied. During each transmission, some intermediate results e.g. the histogram of the soft bits at the input- and output of the LDPC decoder and the currently measured throughput can be shown. After all transmissions are finished, the results will be evaluated and saved.

6.3.5 HIL-Measurement Results

In the HIL test, OFDM signals with 256 subcarriers and CP length of 32 samples were transmitted. In the non-sharing case, each operator transmits in half of the available spectrum using a normal DF relaying scheme. The transmission bandwidth was about 125 MHz. Rayleigh channels with 16 taps were used. The carrier frequency of 2.4 GHz.

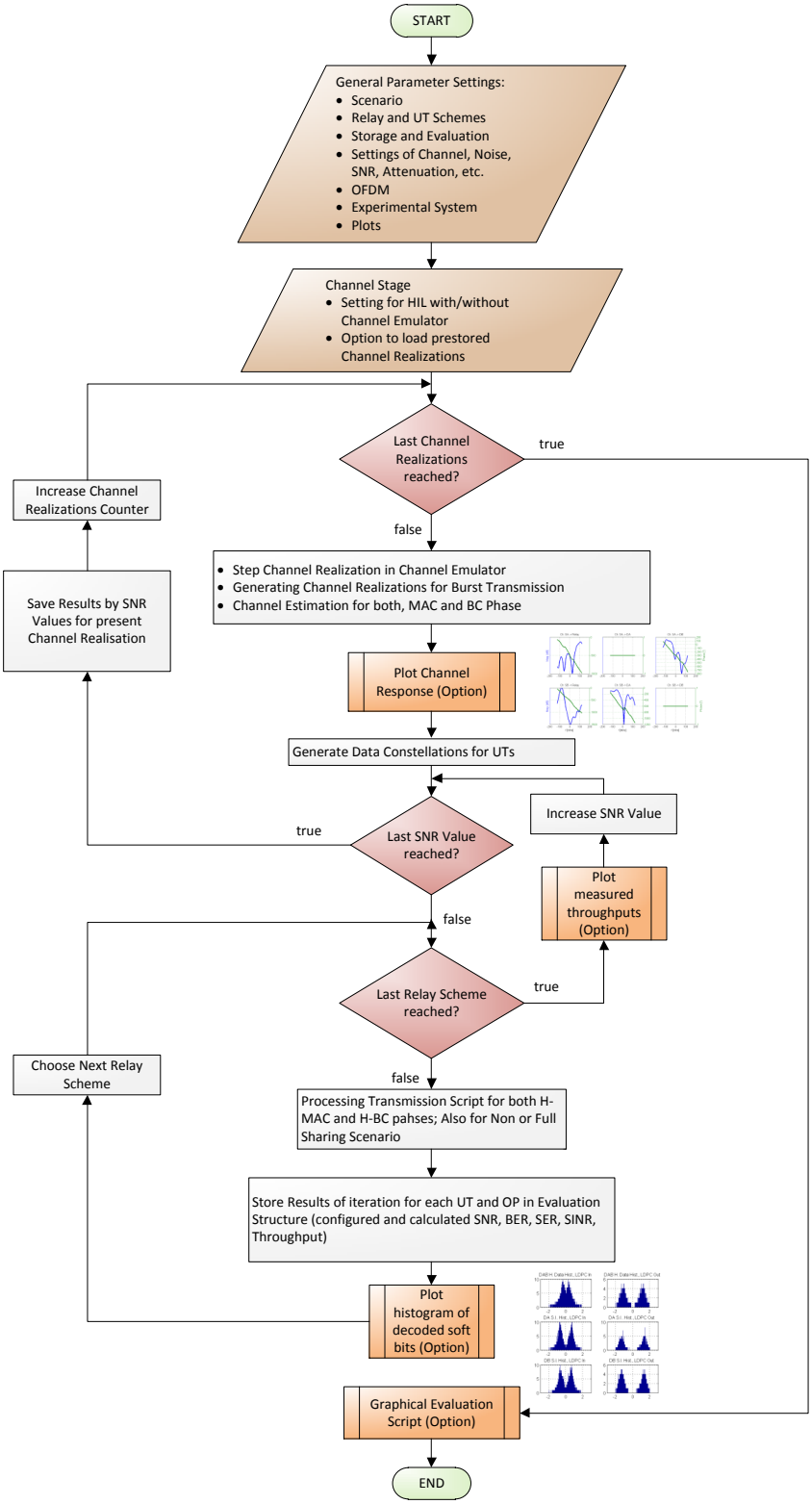

Figure 6.41: Flowchart of the software implementation of the relay sharing scenario with “butterfly” network.

6.3.5.1 HIL-Measurements using Rayleigh Channels and Cable Network Mode

Figure 6.42, Figure 6.43 and Figure 6.44 show the coded sum rates of the non-sharing case and the AF-SIC- and HDF strategies, respectively. As shown, without sharing, the sum rate is relatively low i.e. with a maximum of 0.17 bits/s/Hz. In both sharing cases, the maximum sum rate has achieved 0.35 bits/s/Hz. Note that the maximum sum rate is limited by the BPSK modulation. Thus, after the SNR has achieved a certain value, the sum rate remains constant in spite of further SNR increase.

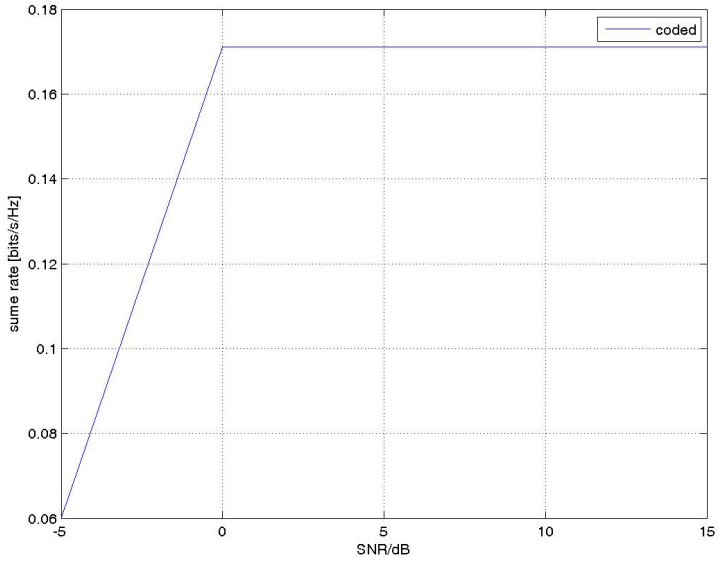

Figure 6.42: Reference scenario: coded sum rate of non-sharing case.

Figure 6.45 and Figure 6.46 show the coded sum rate difference between the AF-SIC- as well as the HDF and the non-sharing case, respectively. As shown, the AF-SIC only has higher coded sum rate than the non-sharing case in about half of the investigated SNR region. In contrast, the HDF has higher coded sum rate than the non-sharing case in about $\frac{2}{3}$ of the total SNR region. These results prove that with spectrum sharing as well as applying the suitable sharing techniques, higher sum rate can be achieved. In other words, the SAPHYRE-gain is shown by these results.

Now, we compare the performance of both relaying strategies. Figure 6.47 shows the sum capacity in bits/symbol of the AF-SIC and HDF with uncoded and coded transmission in different SNR regions. As shown, with uncoded transmission, the areas of the full sum capacity SNR regions of HDF and AF-SIC are similar. However, with coded transmission, full sum capacity SNR region of HDF is much larger than that of AF-SIC.

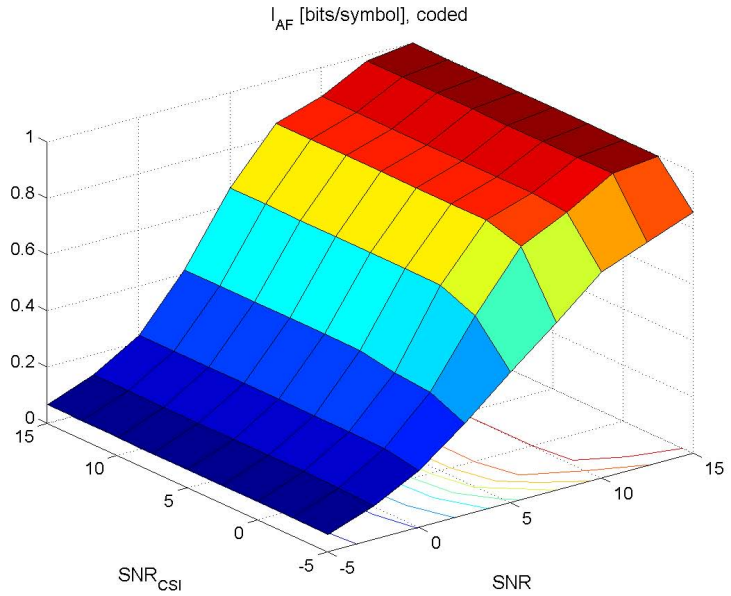

Figure 6.43: Scenario S1-TC-I: coded sum rate of AF-SIC strategy with spectrum sharing.

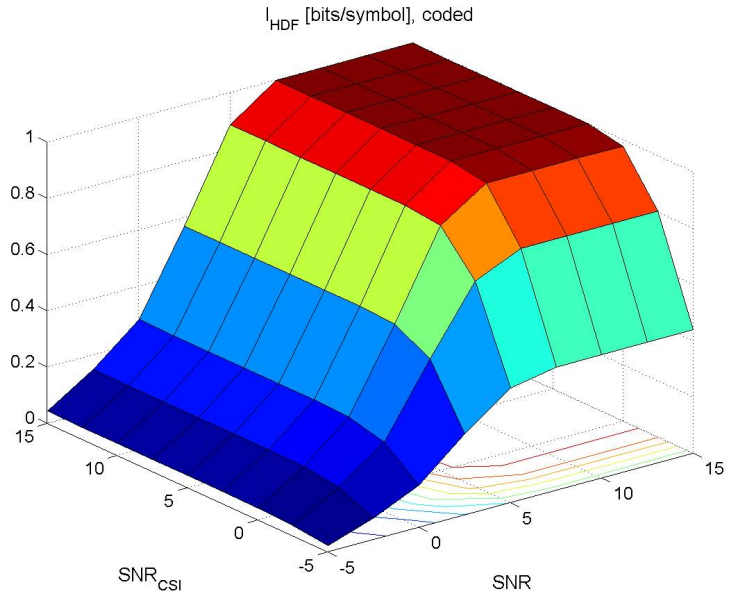

Figure 6.44: Scenario S1-TC-I: coded sum rate of HDF strategy with spectrum sharing.

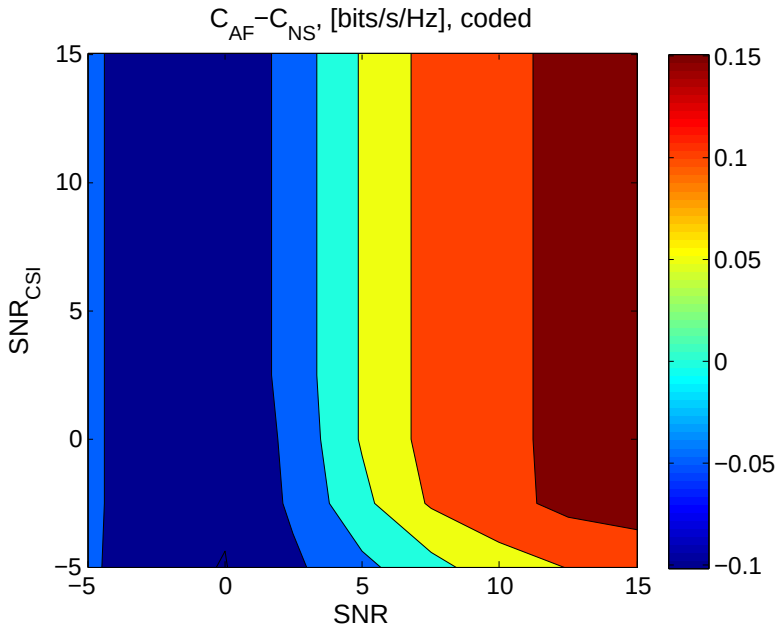

Figure 6.45: Scenario S1-TC-I: coded sum rate difference between AF-SIC and the non-sharing case.

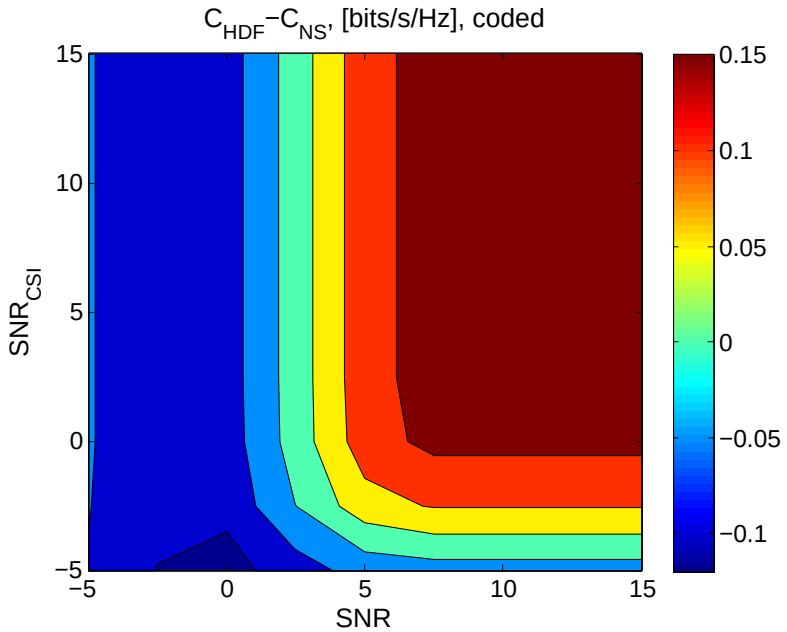

Figure 6.46: Scenario S1-TC-I: coded sum rate difference between HDF and the non-sharing case.

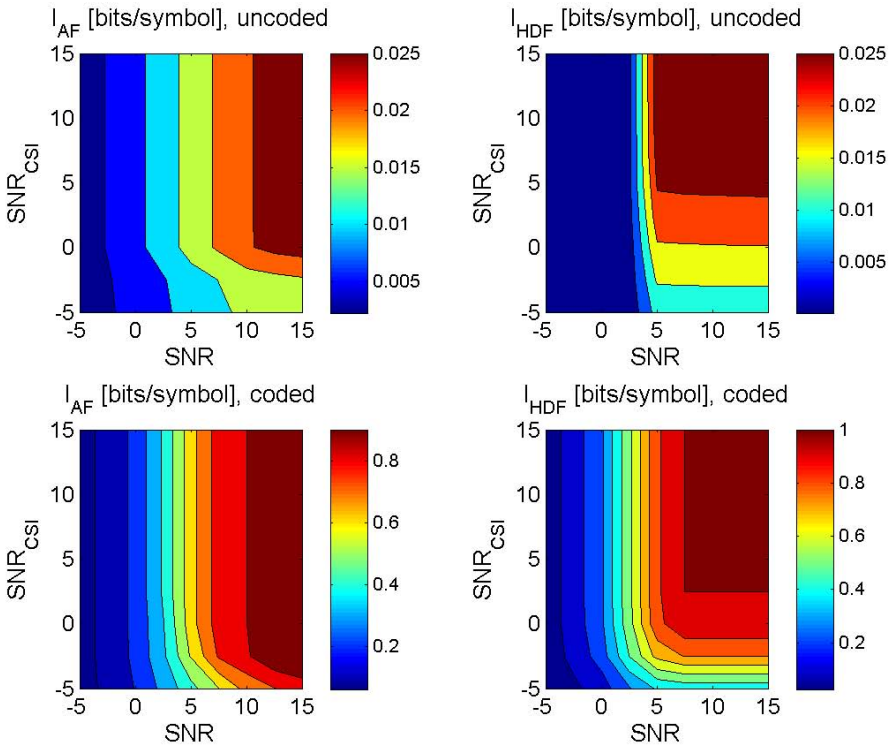

Figure 6.47: Scenario SC1-TC-I: capacity of HDF and AF-SIC with uncoded and coded transmission in different SNR regions.

Figure 6.48 and Figure 6.49 show the sum capacity difference between both techniques and the non-sharing case. As shown, in the uncoded case, HDF only has advantage against AF-SIC for a relatively small range of SNR and relatively large SNR_{CSI}. In contrast, with coded transmission, HDF has better performance than AF-SIC in the major part of the investigated SNR region (which is realistic). Only with very low SNR of C-SI and relatively high SNR of the MAC- and BC links, AF-SIC has considerable advantage over HDF. Thus, we can conclude that in the coded case, the HDF is more robust than AF-SIC for the observed resource sharing scenario.

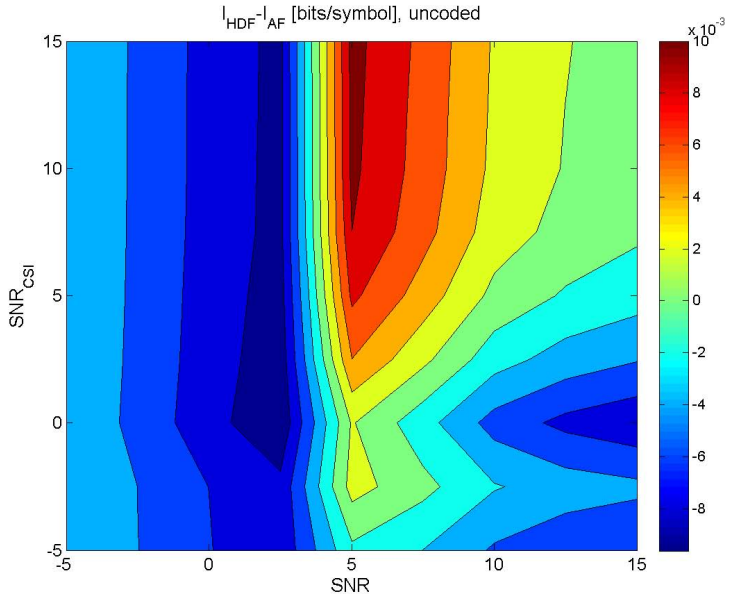

Figure 6.48: Scenario SC1-TC-I: capacity difference of HDF and AF-SIC with uncoded transmission in different SNR regions.

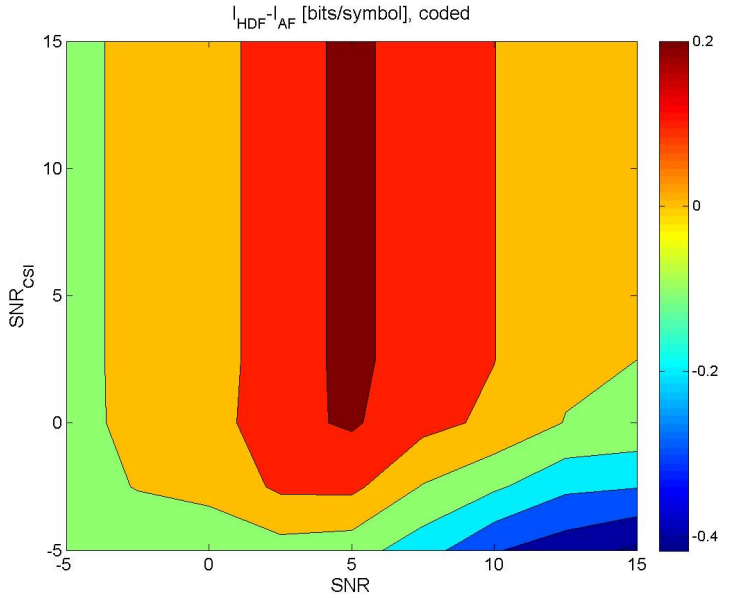

Figure 6.49: Scenario SC1-TC-I: capacity difference of HDF and AF-SIC in coded transmission in different SNR regions.

6.3.5.2 HIL-Measurements using Rayleigh Channels in Channel Emulator

In this HIL test, we investigate the following three cases of SNR regions in detail: high SNR (about 15 dB), medium SNR (about 8 dB) and low SNR (about 0 dB). These different SNR regions are achieved by adjusting the Tx power. For reference, Fig. 6.50 shows the channel frequency response in the H-BC phase, which was estimated with high SNR.

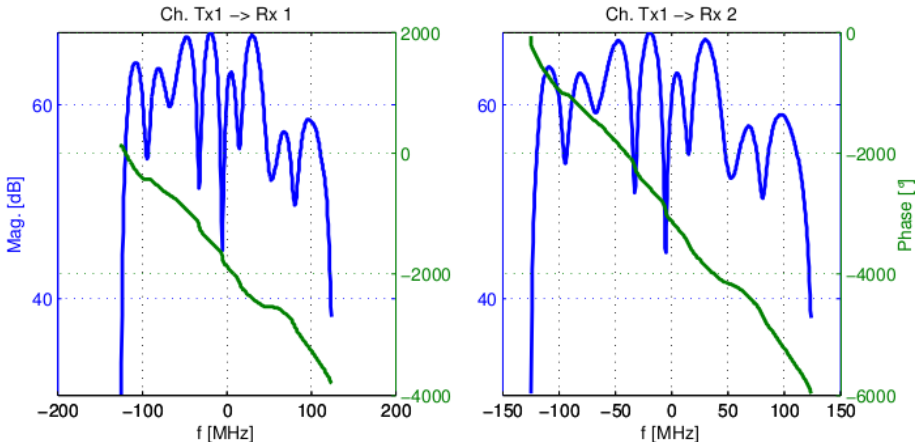

Figure 6.50: Channel frequency response in the H-BC phase of scenario SC1-TC-I.

Fig. 6.51 ∼ Fig. 6.54 show the measured capacity of both proposed schemes and the corresponding histogram of the soft bits in different phases in the high SNR case. As

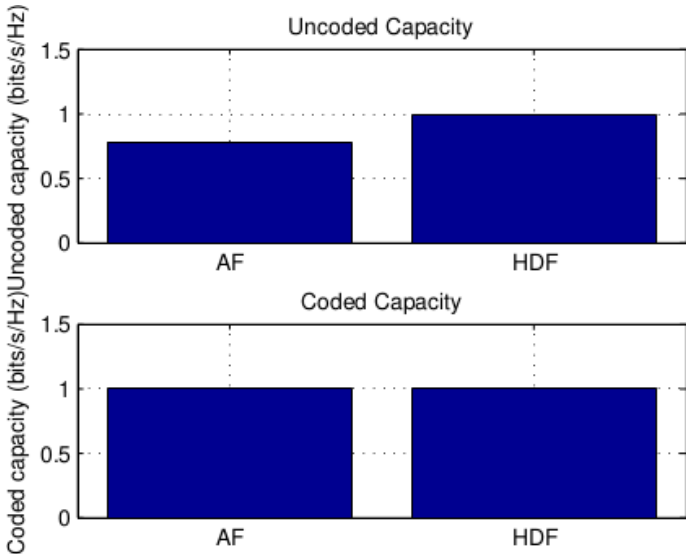

Figure 6.51: Measured capacity of both HDF and AF schemes in uncoded and coded cases. High SNR.

shown in Fig. 6.51, with high SNR, HDF only outperforms AF-SIC in the uncoded case. With the coding gain by the LDPC code, the capacity of both schemes become the same. This implies that with high SNR, the LDPC code can sufficiently reduce the interference caused by spectrum sharing in the AF-SIC scheme.

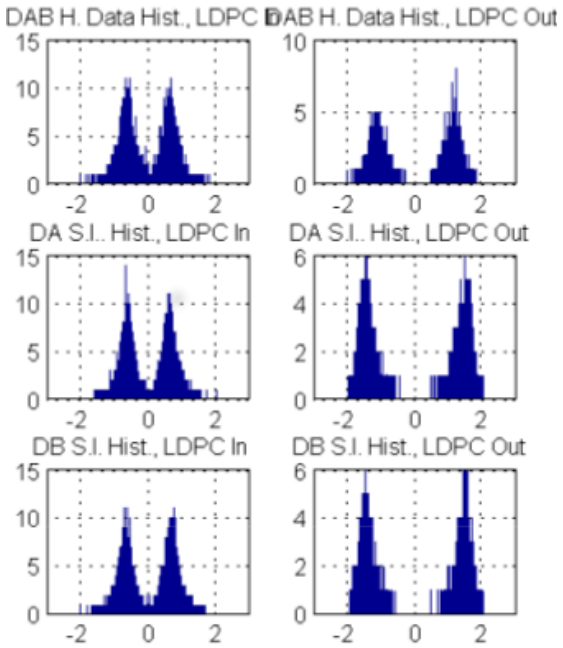

Figure 6.52: Histogram of the soft bits before and after LDPC decoding in the HMAC phase, including the hierarchical bits of the HDF scheme and the C-SI bits. High SNR.

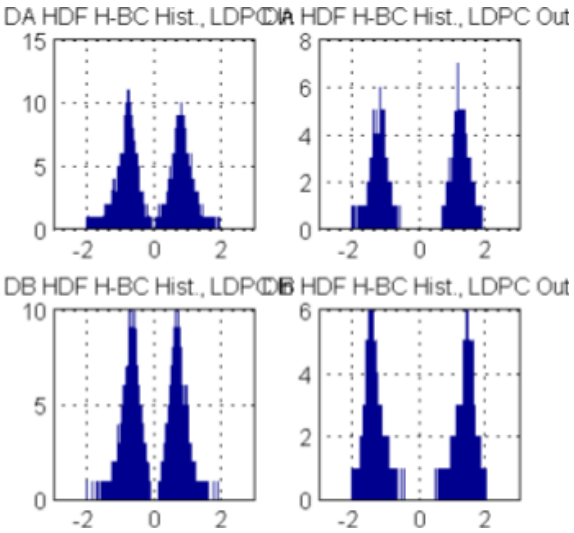

Figure 6.53: Histogram of the soft bits of the HDF scheme before and after LDPC decoding in the HBC phase. High SNR.

However, by comparing Fig. 6.53 and Fig. 6.54, we can see that HDF achieves lower residual error level than AF-SIC. This means that if higher order modulation is used (assuming the corresponding HDF scheme exists), the HDF scheme will outperform the AF-SIC scheme.

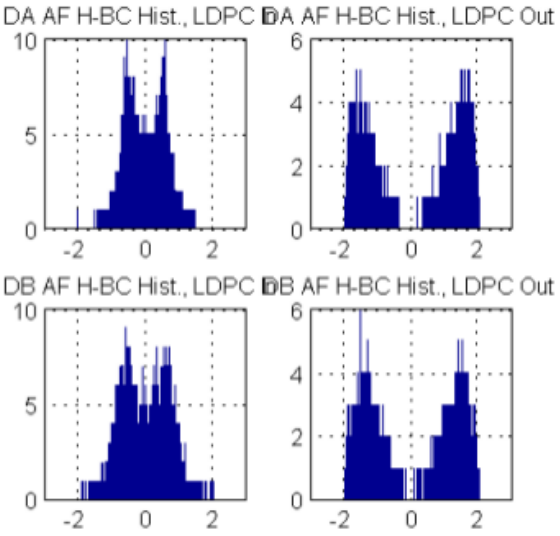

Figure 6.54: Histogram of the soft bits of the AF scheme before and after LDPC decoding in the HBC phase. High SNR.

Fig. 6.55 $\sim$ Fig. 6.58 show the measured capacity of both proposed schemes and the corresponding histogram of the soft bits in different phases in the medium SNR case. As shown in Fig. 6.55, with medium SNR, HDF outperforms AF-SIC in both uncoded and coded cases. By comparing Fig. 6.57 and Fig. 6.58, we can see that

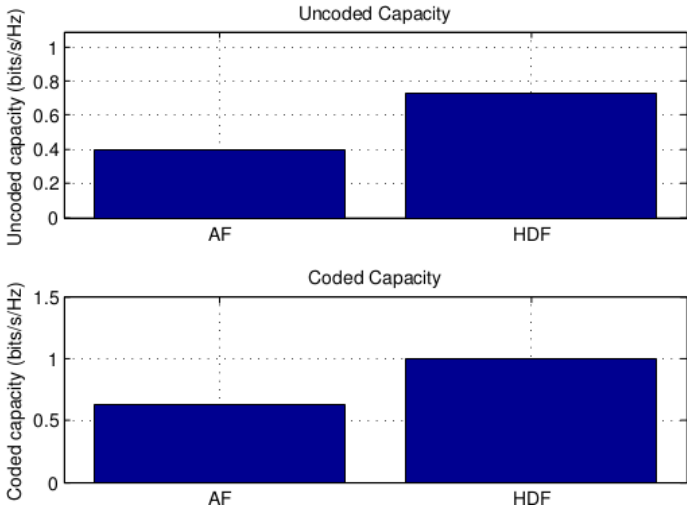

Figure 6.55: Measured capacity of both HDF and AF schemes in uncoded and coded cases. Medium SNR.

HDF achieves almost interference free decoding, while AF-SIC suffers from residual interference caused by spectrum sharing, which can not be suppressed by the LDPC code in such an SNR region.

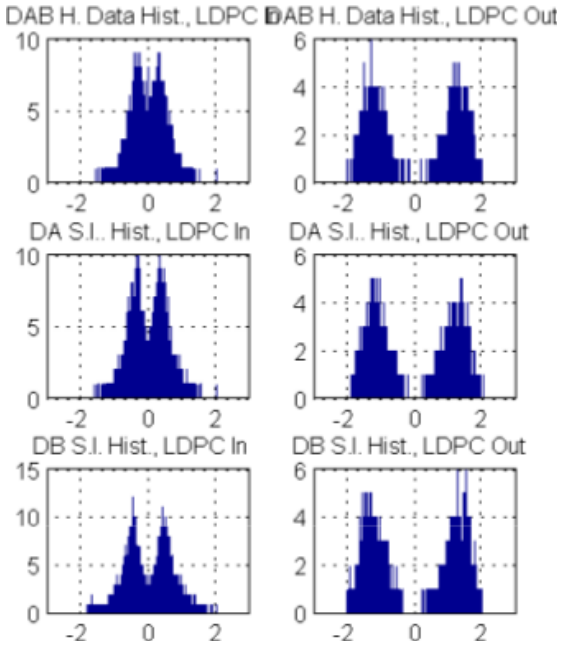

Figure 6.56: Histogram of the soft bits before and after LDPC decoding in the HMAC phase, including the hierarchical bits of the HDF scheme and the C-SI bits. Medium SNR.

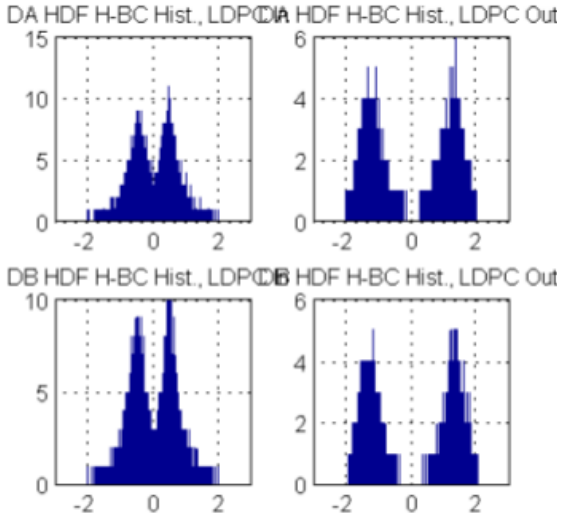

Figure 6.57: Histogram of the soft bits of the HDF scheme before and after LDPC decoding in the HBC phase. Medium SNR.

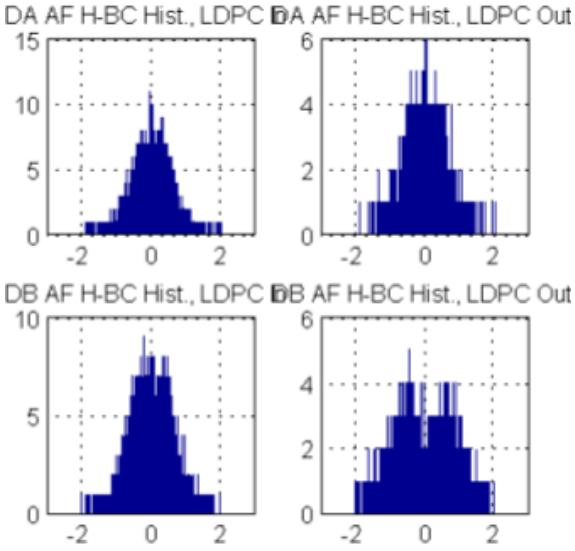

Figure 6.58: Histogram of the soft bits of the AF scheme before and after LDPC decoding in the HBC phase. Medium SNR.

Fig. 6.59 $\sim$ Fig. 6.62 show the measured capacity of both proposed schemes and the corresponding histogram of the soft bits in different phases in the low SNR case. As shown in Fig. 6.59, with low SNR, both HDF and AF schemes achieve only very low capacity. While AF outperforms HDF in the uncoded case, HDF slightly outperforms AF-SIC in coded cases. The strong noise can corrupt both the hierarchical decoding and the LDPC decoding.

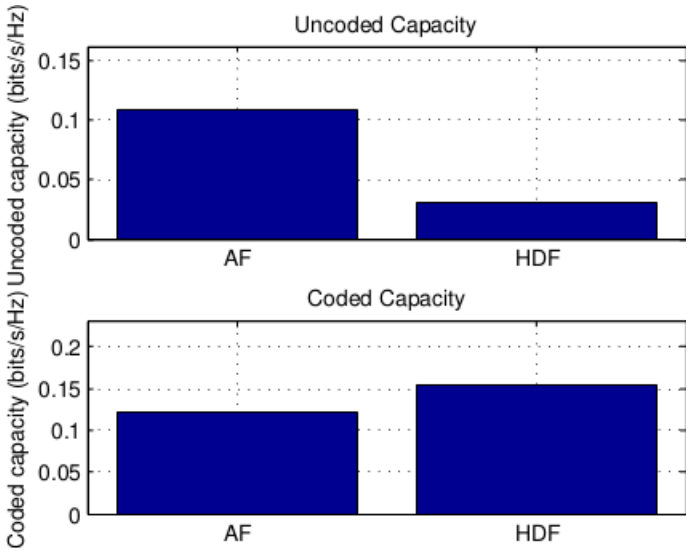

Figure 6.59: Measured capacity of both HDF and AF schemes in uncoded and coded cases. Low SNR.

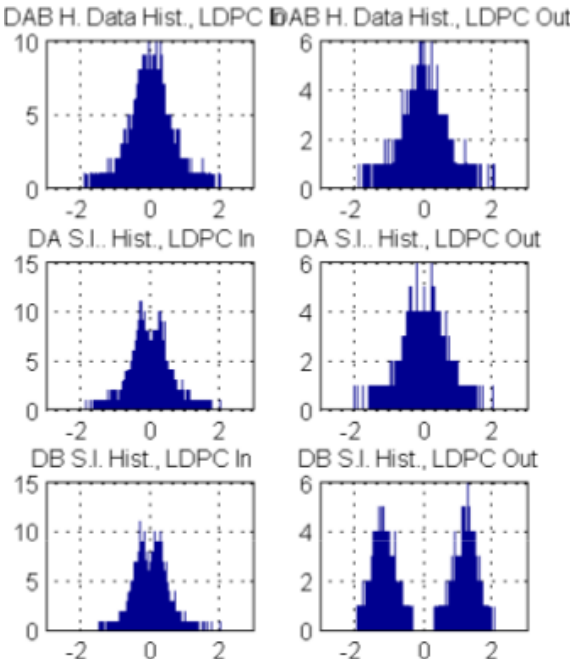

Figure 6.60: Histogram of the soft bits before and after LDPC decoding in the HMAC phase, including the hierarchical bits of the HDF scheme and the C-SI bits. Low SNR.

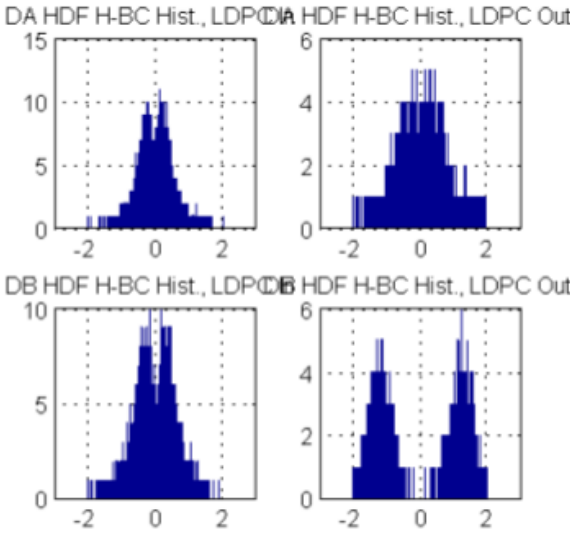

Figure 6.61: Histogram of the soft bits of the HDF scheme before and after LDPC decoding in the HBC phase. Low SNR.

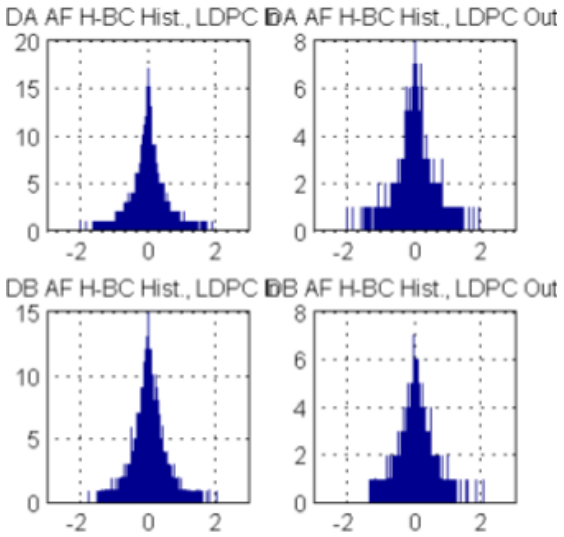

Figure 6.62: Histogram of the soft bits of the AF scheme before and after LDPC decoding in the HBC phase. Low SNR.

Finally, we can conclude that the advantage of the HDF scheme is mostly in the medium SNR region. Actually, Fig. 6.49 already shew that in a large area of SNR region of the coded case, the HDF scheme either outperforms the AF-SIC scheme or has the same performance. Thus, the HDF scheme is favorable. However, we should consider that the AF-SIC scheme outperforms the HDF scheme in very low SNR region or in the cases with very bad C-SI. Also, in the uncoded case, the AF-SIC scheme also has a quite large SNR region where it outperforms the HDF scheme. Thus, the choice of the schemes indeed depends on the operating SNR region. The ideal case will be an adaptive switch between both schemes according to SNR of the direct links and that of the C-SI links.

6.4 Scenario SC1-TC-II: Relay Sharing in Two-Way-Relaying Network

6.4.1 Scenario and Test Case Description

6.4.1.1 Scenario Description

Figure 6.63 describes a Two-Way-Relaying (TWR) scenario with both relay and spectrum sharing by two different operators. In this scenario, multiple communication partners (owned by different operators) use one relay station (possibly owned by another operator/virtual operator) to bidirectionally exchange information using a shared spectrum. In our investigation, one communication partner is a BS and a UT of one operator. Furthermore, the direct link between a BS and its dedicated UT is blocked, e.g. by a high building. This happens in typical urban area.

Therefore, the use of the relay station for data exchange is necessary. We assume that all BS's and UT's as well as the relay station have multiple antennas and operate in half-duplex mode. The TWR consists of two phase: the MAC-phase and the BC-phase. In the MAC-phase, all BS's and UT's transmit data to the relay. In the BC-phase, the relay broadcast data to all BS's and UT's. This broadcast data was calculated by the relay according to its received data in the MAC-phase. The relay station must take into account the fact that multiple operators are active and manage the interference they cause to each other according to their voluntary agreements.

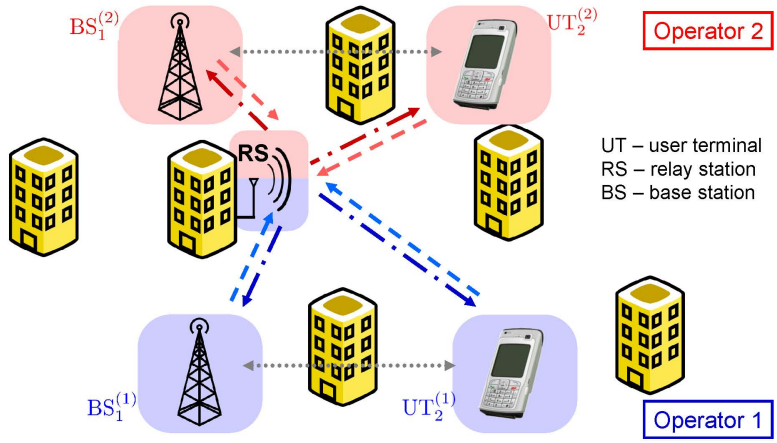

Figure 6.63: Scenario SC1-TC-II: Two Way Relaying (TWR) with multiple links of different operators sharing both the relay and the spectrum.

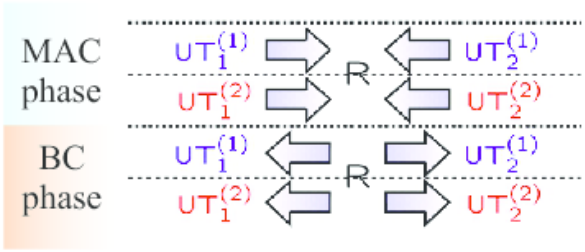

Figure 6.64: Scenario SC1-TC-II: Illustration of the MAC- and BC phases of the TWR procedure.

6.4.1.2 Test Case Description

For the test of this scenario on the demonstrator platform, we set the numbers of both Tx/Rx antennas at the relay to be 4. All UT have only single Tx and Rx antennas, respectively. OFDM is applied as the PHY technique. The total number

of non-zero subcarriers and NULL subcarriers can be flexible. The length of the CP can also be flexible. Since no LTE measurements have been done for this scenario, Rayleigh channels are used. Different digital modulation waveforms can be applied e.g. BPSK, QPSK etc.

In this scenario, the following comparisons and investigations should be made:

- To verify the spectrum sharing gain in this TWR scenario and network configuration, the case with spectrum sharing should be compared with the case without spectrum sharing. In the case with spectrum sharing, all operators transmit signals in on the same frequency. Thus, enabling techniques should be applied to mitigate the interference between different operators and maximize the throughput/data rate. In the case without spectrum sharing case, each operator uses a half of the available frequency band, i.e. they have orthogonal spectrum. In each spectrum, they apply advanced multi-antenna signal processing technique at the relay.
- In the case of spectrum sharing, different enabling relay signal processing techniques (algorithms) should be compared. With such comparison, we can identify the advantages and disadvantages of the different techniques and can choose the most appropriate technique for deployment.

The used performance metrics in our HIL tests include: sum rate (in bits/s/Hz), single user (operator) rate (in bits/s/Hz) and throughput (in bits/s/Hz).

6.4.2 Enabling Algorithms

6.4.2.1 System Model

The system model is derived from the scenario depicted in Fig. 6.63 and Fig. 6.64. We assume that pairs of users belonging to the same operator would like to communicate with each other. Therefore, the relay station must take into account the fact that multiple operators are active and manage the interference they cause to each other according to their voluntary agreements. The relay is equipped with M_{R} antennas and uses amplify and forward two-way relaying. Moreover, the k-th terminal belonging to the ℓ-th operator has $M_k^{(\ell)}$ antennas.

The traditional solution to avoid inter-operator interference is to assign orthogonal resources to the two groups, e.g. different frequencies (FDMA) or different time slots (TDMA). Consequently, for each group, any single-operator two-way relaying techniques can be applied, e.g. the algebraic norm-maximizing transmit strategy (ANOMAX) and Rank-Restored ANOMAX (RRANOMAX) [32]. This corresponds to the case of exclusive frequency bands and physically separated infrastructure. However, by using this scheme the individual sum data rate of each operator decreases by a factor of two since the time slots have to be shared. Therefore, in order to investigate the potential gain from voluntary infrastructure sharing, we propose

an SDMA-based approach that allows both operators to serve their users via a physically shared relay by taking advantage of multiple antennas at the relay. This implies that the operators agree to voluntarily share their infrastructure and their spectrum in a coordinated manner. As we demonstrate, this form of cooperation not only reduces the operators' expenditure but additionally provides them with an improvement in the overall sum rate, since the resources are used more efficiently. These benefits provide the motivation for the operators to share their spectrum as well as their infrastructure. Our procedure consists of two steps. In the first step, the system is converted into two parallel independent sub-systems. Then, in the second step, arbitrary transmission techniques for single-operator two-way relaying can be applied. Note that this two-step approach is used here only for simplicity since it is in general suboptimal.

As in the basic two-way relaying scenario, where two users exchange data with the help of one relay, all belonging to a single operator [32], the transmission takes place in two phases. In the first phase, each terminal transmits to the relay using the same resources, so that their transmissions interfere. Assuming frequency-flat fading and denoting the channel between the k-th user of the ℓ-th operator and the relay by $\boldsymbol{H}_k^{(\ell)} \in \mathbb{C}^{M_\mathrm{R} \times M_k^{(\ell)}}$, where $k, \ell \in \{1, 2\}$, the signal received by the relay can be expressed as

$$\boldsymbol{r} = \boldsymbol{H}^{(1)} \cdot \boldsymbol{x}^{(1)} + \boldsymbol{H}^{(2)} \cdot \boldsymbol{x}^{(2)} + \boldsymbol{n}_\mathrm{R} \in \mathbb{C}^{M_\mathrm{R} \times 1}, \tag{6.5}$$

where $\boldsymbol{H}^{(\ell)} = \left[\boldsymbol{H}_1^{(\ell)}, \boldsymbol{H}_2^{(\ell)}\right]$ represents the concatenated MIMO channel of the ℓ-th operator, $\boldsymbol{x}^{(\ell)} = \left[\boldsymbol{x}_1^{(l)^\mathrm{T}}, \boldsymbol{x}_2^{(l)^\mathrm{T}}\right]^\mathrm{T}$ is the aggregate transmitted signal from each operator, and the vector $\boldsymbol{n}_\mathrm{R}$ is the noise component at the relay. Moreover, to simplify the notation, we assume that reciprocity is valid so that the backward channel between the relay and the k-th user of the ℓ-th operator is given by $\boldsymbol{H}_k^{(\ell)^\mathrm{T}}$. This assumption is fulfilled in a TDD system if identical RF chains are applied.

In the second transmission phase, the relay transmits to all terminals simultaneously. Since we assume an amplify and forward relay, the signal transmitted by the relay can be expressed as

$$\bar{\boldsymbol{r}} = \gamma \cdot \boldsymbol{G} \cdot \boldsymbol{r} \quad \text{for} \quad \boldsymbol{G} = \gamma_0 \cdot \boldsymbol{G}_\mathrm{T} \cdot \boldsymbol{G}_\mathrm{S} \cdot \boldsymbol{G}_\mathrm{R}. \tag{6.6}$$

Here, the parameter $\gamma_0 \in \mathbb{R}^+$ is chosen such that the relay amplification matrix $\boldsymbol{G} \in \mathbb{C}^{M_\mathrm{R} \times M_\mathrm{R}}$ is normalized to unit Frobenius norm. Moreover, $\gamma \in \mathbb{R}^+$ is the scaling factor used for adjusting the signal so that the transmit power constraint is fulfilled. The matrices $\boldsymbol{G}_\mathrm{T} \in \mathbb{C}^{M_\mathrm{R} \times 2M_\mathrm{R}}$ and $\boldsymbol{G}_\mathrm{R} \in \mathbb{C}^{2M_\mathrm{R} \times M_\mathrm{R}}$ represent the relay's receive filter and transmit filter, respectively. Their task is to mitigate the inter-operator interference for each sub-system. The matrix $\boldsymbol{G}_\mathrm{S} \in \mathbb{C}^{2M_\mathrm{R} \times 2M_\mathrm{R}}$ is constructed via

$$\boldsymbol{G}_\mathrm{S} = \begin{bmatrix} \boldsymbol{G}_\mathrm{S}^{(1)} & \boldsymbol{0}_{M_\mathrm{R} \times M_\mathrm{R}} \\ \boldsymbol{0}_{M_\mathrm{R} \times M_\mathrm{R}} & \boldsymbol{G}_\mathrm{S}^{(2)} \end{bmatrix}, \tag{6.7}$$

where $\boldsymbol{G}_{\mathrm{S}}^{(1)}, \boldsymbol{G}_{\mathrm{S}}^{(2)} \in \mathbb{C}^{M_{\mathrm{R}} \times M_{\mathrm{R}}}$ are the relay amplification matrices for each sub-system. Note that $\boldsymbol{G}_{\mathrm{S}}$ is block diagonal since it represents the processing performed in the individual subsystems.

The transmit and receive filter matrices $\boldsymbol{G}_{\mathrm{T}}$ and $\boldsymbol{G}_{\mathrm{R}}$ can also be partitioned as

$$\boldsymbol{G}_{\mathrm{T}} = \left[\boldsymbol{G}_{\mathrm{T}}^{(1)}, \quad \boldsymbol{G}_{\mathrm{T}}^{(2)}\right] \text{ and } \boldsymbol{G}_{\mathrm{R}} = \left[\boldsymbol{G}_{\mathrm{R}}^{(1)^{\mathrm{T}}}, \quad \boldsymbol{G}_{\mathrm{R}}^{(2)^{\mathrm{T}}}\right]^{\mathrm{T}}, \tag{6.8}$$

where $\boldsymbol{G}_{\mathrm{T}}^{(\ell)} \in \mathbb{C}^{M_{\mathrm{R}} \times M_{\mathrm{R}}}$ and $\boldsymbol{G}_{\mathrm{R}}^{(\ell)} \in \mathbb{C}^{M_{\mathrm{R}} \times M_{\mathrm{R}}}$ for $\ell \in \{1, 2\}$.

After establishing the system model, in the next section, we focus on the question how to find the matrices $\boldsymbol{G}_{\mathrm{T}}$, $\boldsymbol{G}_{\mathrm{S}}$, and $\boldsymbol{G}_{\mathrm{R}}$.

6.4.2.2 Two-step algorithm

The separation of the the two sub-systems requires the suppression of the inter-operator interference. The scheme we propose here is inspired by the precoding technique BD that was first proposed in [24]. Via BD we force all the inter-operator interference to zero by choosing one operator's relay receive filter matrix $\boldsymbol{G}_{\mathrm{R}}^{(\ell_1)}$ such that it projects the signal into the null space of the other operator's channel matrices $\boldsymbol{H}^{(\ell_2)}$ for $\ell_1 \neq \ell_2$ and $\ell_1, \ell_2 \in \{1, 2\}$. Thereby, the received signal at the relay is decomposed into two parallel independent sub-systems. The projection matrix can for example be calculated from the SVD of $\boldsymbol{H}^{(\ell_2)}$, as in BD [24]. To ensure that the system seen by the users of each operator in the second transmission phase is also isolated from the inter-operator interference, the transmit filter matrix $\boldsymbol{G}_{\mathrm{T}}$ for the second ("downlink") phase needs to be applied. Due to the reciprocity of the channel, we can simply choose $\boldsymbol{G}_{\mathrm{T}} = \boldsymbol{G}_{\mathrm{R}}^{\mathrm{T}}$. However, we should be aware that the BD algorithm has a dimensionality constraint stating that the total accumulated number of antennas at each user terminal has to be less or equal than the number of antennas at the relay.

After canceling the interference between the operators, the overall received signal in the downlink can be expressed as

$$\begin{aligned}
\begin{bmatrix} \boldsymbol{y}^{(1)} \\ \boldsymbol{y}^{(2)} \end{bmatrix} &= \gamma \cdot \gamma_0 \cdot \begin{bmatrix} \boldsymbol{H}^{(1)^{\mathrm{T}}} \\ \boldsymbol{H}^{(2)^{\mathrm{T}}} \end{bmatrix} \cdot \boldsymbol{G}_{\mathrm{T}} \cdot \boldsymbol{G}_{\mathrm{S}} \cdot \boldsymbol{G}_{\mathrm{R}} \cdot \left[\boldsymbol{H}^{(1)} \boldsymbol{H}^{(2)}\right] \cdot \begin{bmatrix} \boldsymbol{x}^{(1)} \\ \boldsymbol{x}^{(2)} \end{bmatrix} + \begin{bmatrix} \tilde{\boldsymbol{n}}^{(1)} \\ \tilde{\boldsymbol{n}}^{(2)} \end{bmatrix} \\
&= \gamma \cdot \gamma_0 \cdot \begin{bmatrix} \boldsymbol{H}^{(1)^{\mathrm{T}}} \cdot \boldsymbol{G}_{\mathrm{R}}^{(1)^{\mathrm{T}}} \cdot \boldsymbol{G}_{\mathrm{S}}^{(1)} \cdot \boldsymbol{G}_{\mathrm{R}}^{(1)} \cdot \boldsymbol{H}^{(1)} & \boldsymbol{0} \\ \boldsymbol{0} & \boldsymbol{H}^{(2)^{\mathrm{T}}} \cdot \boldsymbol{G}_{\mathrm{R}}^{(2)^{\mathrm{T}}} \cdot \boldsymbol{G}_{\mathrm{S}}^{(2)} \cdot \boldsymbol{G}_{\mathrm{R}}^{(2)} \cdot \boldsymbol{H}^{(2)} \end{bmatrix} \\
&\quad \cdot \begin{bmatrix} \boldsymbol{x}^{(1)} \\ \boldsymbol{x}^{(2)} \end{bmatrix} + \begin{bmatrix} \tilde{\boldsymbol{n}}^{(1)} \\ \tilde{\boldsymbol{n}}^{(2)} \end{bmatrix},
\end{aligned} \tag{6.9}$$

where $\boldsymbol{y}^{(\ell)} \in \mathbb{C}^{(M_1^{(\ell)} + M_2^{(\ell)}) \times 1}$ and $\tilde{\boldsymbol{n}}^{(\ell)} \in \mathbb{C}^{(M_{(\ell)}^{l} + M_2^{(\ell)}) \times 1}$ are the signal and the effective noise term received by operator ℓ. Consequently, for each sub-system we obtain

$$\boldsymbol{y}^{(\ell)} = \gamma \cdot \gamma_0 \cdot \tilde{\boldsymbol{H}}^{(\ell)^{\mathrm{T}}} \cdot \boldsymbol{G}_{\mathrm{S}}^{(\ell)} \cdot \tilde{\boldsymbol{H}}^{(\ell)} \cdot \boldsymbol{x}^{(\ell)} + \tilde{\boldsymbol{n}}^{(\ell)}, \tag{6.10}$$

Table 6.1: Comparison of Relay Amplification Schemes

Algorithm	$\boldsymbol{G}_{\mathrm{T}}$	$\boldsymbol{G}_{\mathrm{S}}$	$\boldsymbol{G}_{\mathrm{R}}$
ZF [34]	$(\boldsymbol{H}^{\mathrm{T}})^{\mathrm{H}}\left((\boldsymbol{H}^{\mathrm{T}})(\boldsymbol{H}^{\mathrm{T}})^{\mathrm{H}}\right)^{-1}$	$\boldsymbol{I}_2 \otimes \left(\boldsymbol{\Pi}_2 \otimes \boldsymbol{I}_{M_k^{(\ell)}}\right)$	$\left((\boldsymbol{H})^{\mathrm{H}}(\boldsymbol{H})\right)^{-1}(\boldsymbol{H})^{\mathrm{H}}$
MMSE [34]	$\left(\boldsymbol{H}^{\mathrm{H}^{\mathrm{T}}}\boldsymbol{H}^{\mathrm{T}} + 4\sigma_k^{(\ell)^2}\boldsymbol{I}_{M_{\mathrm{R}}}/P_{\mathrm{R}}\right)^{-1}\boldsymbol{H}^{\mathrm{H}^{\mathrm{T}}}$	$\boldsymbol{I}_2 \otimes \left(\boldsymbol{\Pi}_2 \otimes \boldsymbol{I}_{M_k^{(\ell)}}\right)$	$\boldsymbol{H}^{\mathrm{H}}\left(\boldsymbol{H}\boldsymbol{H}^{\mathrm{T}} + \sigma_{\mathrm{R}}^2\boldsymbol{I}_{M_{\mathrm{R}}}/P_k^{(\ell)}\right)^{-1}$
ProBaSeMO (BD)	$\boldsymbol{G}_{\mathrm{R}}^{\mathrm{T}}$	Arbitrary block diagonal matrix	$\tilde{\boldsymbol{U}}_{\mathrm{n}}^{(\ell)}\tilde{\boldsymbol{U}}_{\mathrm{n}}^{(\ell)^{\mathrm{H}}}\forall\ell$
ProBaSeMO (RBD)	$\tilde{\boldsymbol{U}}^{(\ell)^*}\left(\tilde{\boldsymbol{\Sigma}}^{(\ell)^*}\tilde{\boldsymbol{\Sigma}}^{(\ell)^{\mathrm{T}}} + 4M_k^{(\ell)}\sigma_k^{(\ell)^2}\boldsymbol{I}_{M_{\mathrm{R}}}/P_{\mathrm{R}}\right)^{-1/2}, \forall\ell$	Arbitrary block diagonal matrix	$\left(P_k^{(\ell)}\tilde{\boldsymbol{\Sigma}}^{(\ell)}\tilde{\boldsymbol{\Sigma}}^{(\ell)^{\mathrm{H}}}/M_k^{(\ell)} + \sigma_{\mathrm{R}}^2\boldsymbol{I}_{M_{\mathrm{R}}}\right)^{-1/2}\tilde{\boldsymbol{U}}^{(\ell)^{\mathrm{H}}}, \forall\ell$

where the transformed channel matrices per operator are given by $\tilde{\boldsymbol{H}}^{(\ell)} = \boldsymbol{G}_{\mathrm{R}}^{(\ell)} \cdot \boldsymbol{H}^{(\ell)}$.

In order to find a suitable $\boldsymbol{G}_{\mathrm{S}}^{(\ell)}$ for each sub-system, any single-operator two-way relaying technique can be applied to the transformed channels $\tilde{\boldsymbol{H}}^{(\ell)}$, e.g. ZF or MMSE transceive filters [33]. However, in our simulations, we will use the ANOMAX strategy proposed in [32] due to its simplicity and its good performance compared to other single-operator two-way relaying transmit strategies.

The ZF and MMSE solution in [34] can be also obtained using the same routine, i.e. designing $\boldsymbol{G}_{\mathrm{T}}$ and $\boldsymbol{G}_{\mathrm{R}}$ using the ZF and MMSE criteria. Since in these cases all the channels are equalized, the matrix $\boldsymbol{G}_{\mathrm{S}}^{(\ell)} = \boldsymbol{\Pi}_2 \otimes \boldsymbol{I}_{M_k^{(\ell)}}$ is a permutation matrix where $\boldsymbol{\Pi}_2 = \left[\begin{smallmatrix} 0 & 1 \\ 1 & 0 \end{smallmatrix}\right]$ is the exchange matrix which ensures that the user will not receive its own transmitted data. A comparison of different relay transmit strategies is shown in Table 6.1. Note that the ZF algorithm requires that $M_{\mathrm{R}} \geq 4M_k^{(\ell)}$ if the same transmit strategy is used. Further mathematical details and the definition of $\tilde{\boldsymbol{U}}_{\mathrm{n}}^{(\ell)}$, $\tilde{\boldsymbol{U}}^{(\ell)}$, and $\tilde{\boldsymbol{\Sigma}}^{(\ell)}$ are found in [11].

6.4.3 Practical Implementation Issues

Unlike the relay scenario in Ch. 6.3, this scenario requires either perfect reciprocity of the MAC and BC channels or feedback of the channel coefficients, both from the UTs to the relay and from the relay to the UTs. Moreover, the relaying algorithm may require noise power estimates. In the following, the practical implementation issues are described in detail.

6.4.3.1 Imperfect Channel Reciprocity

Originally, the TWR algorithms are designed assuming perfect reciprocity of the MAc and the BC channels. However, the channel reciprocity is hard to fulfill, since the effective channel includes both the radio channel and the transfer functions of the RF chains. Generally, the transfer functions of the Tx- and Rx RF chains are different. Moreover, even if we assume the transfer functions of all RF chains to be identical[9], the received signals at the relay and those at the individual UTs contain different mixtures of the individual channels. The different mixtures result

[9]This has been demonstrated by FhG applying adequate RF calibration techniques.

in different peak position of the mixed channel amplitude, causing difference of signal frame starting point (identified via time synchronization) and thus, phase difference between MAC and BC channels as well as between the different channels associated to the different UTs in the BC phase. This effect destroys the reciprocity of the effective channels (obtained by channel estimation).

The most general and effective solution is to extend the relaying algorithms to the case without channel reciprocity. This is done by feeding back this problem to WP3. With this solution, the transmission will contain an extra BC-phase before the actual data transmission. First, a BC transmission of pilot signals is carried out to estimate the BC channels (and also the noise power at the UTs). Afterwards, the MAC phase pilot and data transmission is carried out, where the MAC channels (and the noise power at the relay) are estimated and the BC channel coefficients are fed back to the relay. Afterwards, the relay calculates the relay matrix based on the channel and noise power estimates. With this relay matrix, the relay transmits the signals in the BC phase. Both the data and the MAC channel estimates have to be sent. Finally, each UT decodes the signals using both the MAC and BC channel estimates.

In the case of assuming identical transfer functions of the RF chains, further simplification is possible to avoid the BC channel estimation. In this case, channel estimation has only to be carried out in the MAC phase. Afterwards, the possible mixtures of channels at the relay in the MAC phase as well as those at different UTs in the BC phase are calculated. With these mixtures, the relations of the peaks of these mixtures can be estimated. Correspondingly, the channel estimates are shifted accordingly for the relay matrix calculation, so that they can match the effective channels in the BC phase.

6.4.3.2 Time Synchronization Error

Except for the difference of channel mixtures mentioned in Sec. 6.4.3.1, time synchronization error can also cause difference of the signal frame starting point. We are planning to integrate additional Rx equalization to solve this problem. Further solutions are under investigation.

6.4.3.3 Colored Noise and Unequal Noise Power

The original designed relaying algorithm has assumed that the noise power at all UTs as well as at the relay is identical. However, this is not realistic. As mentioned before, the noise in practical systems is generally colored and consists narrow band interference. Moreover, the noise characteristic is generally different in different devices. Thus, the noise power values at different UTs and the relays are generally different. Moreover, the noise power values at different subcarriers are also different. Therefore, the relaying algorithm has to take this fact into account. After feeding

this problem back to WP3, the relaying algorithms have been improved and can cope with different noise power at different UTs and at the relay. Finally, we should note that for some of the proposed algorithms, both CSI and noise power information need to be fed back from the UT's to the relay station.

6.4.3.4 Rescaling of the Channel Coefficients or the Noise Power

In the relay, both the MAC and BC channel coefficients are used for the calculation the relaying matrix, which is used to precode the transmit signal of the relay in the BC phase. Similar to scenario SC2-TA and SC1-TB (see also 6.1.3.5), the BC channel for the calculation of the relay matrix has to be rescaled according to the amplitude scaling factor of the transmit signal in the BC phase. However, this scaling factor is unknown until the relay matrix is available. Thus, the same "deadlock" problem as in scenario SC2-TA and SC1-TB (see also 6.1.3.5) exists. Moreover, at each UT, the rescaled BC channel coefficients must be available, since they are further used to separate the desired signal stream from a mixture with the one sent by itself. The solutions in scenario SC2-TA and SC1-TB, i.e. using predefined scaling factor or iterative calculation, can be applied. The rescaling factor should be sent to the UTs, so that they can decode the received signal (in the BC phase). Since this information is the same for all UTs, the corresponding transmission is quite uncomplicated, i.e. with low overhead.

6.4.4 Mapping on the HIL-Demonstrator Platform

For the test of the SC1-TC-II scenario, the relay and the UTs are mapped to the demonstrator platform under the channel emulator mode. Due to the large number of Tx- and Rx antennas (8 Tx-/Rx antennas) compared to the available number on the HIL platform, different mappings are required in MAC and BC phases, as illustrated in Fig. 6.65. In this way, the physical transmitters and receivers can be reused. In the MAC phase, the 4 Tx antennas of the two experimental devices act the 4 single antenna UT's, while the 4 Rx antennas act the receiver of the relay (with 4 Rx antennas). In the BC phase, the roles of the Tx antennas and the Rx antennas are exchanged. The 4 Tx antennas and 4 Rx antennas of the platform are connected to the corresponding inputs and outputs of the channel emulator, respectively. To allow the remapping in the MAC and BC phases, normal channel emulation files can not be used, since they can emulate either the MAC or the BC channels. For the remapping, we need switching of the channels for the transition from MAC to BC or vice versa.

Fig. 6.66 shows the flowchart of the HIL test program. First, general parameter settings are carried out. Afterwards, the channel set up is carried out including the selection of the channel mode and the loading of the channel files. Afterwards, channel realization control and channel estimation are carried out. With each channel

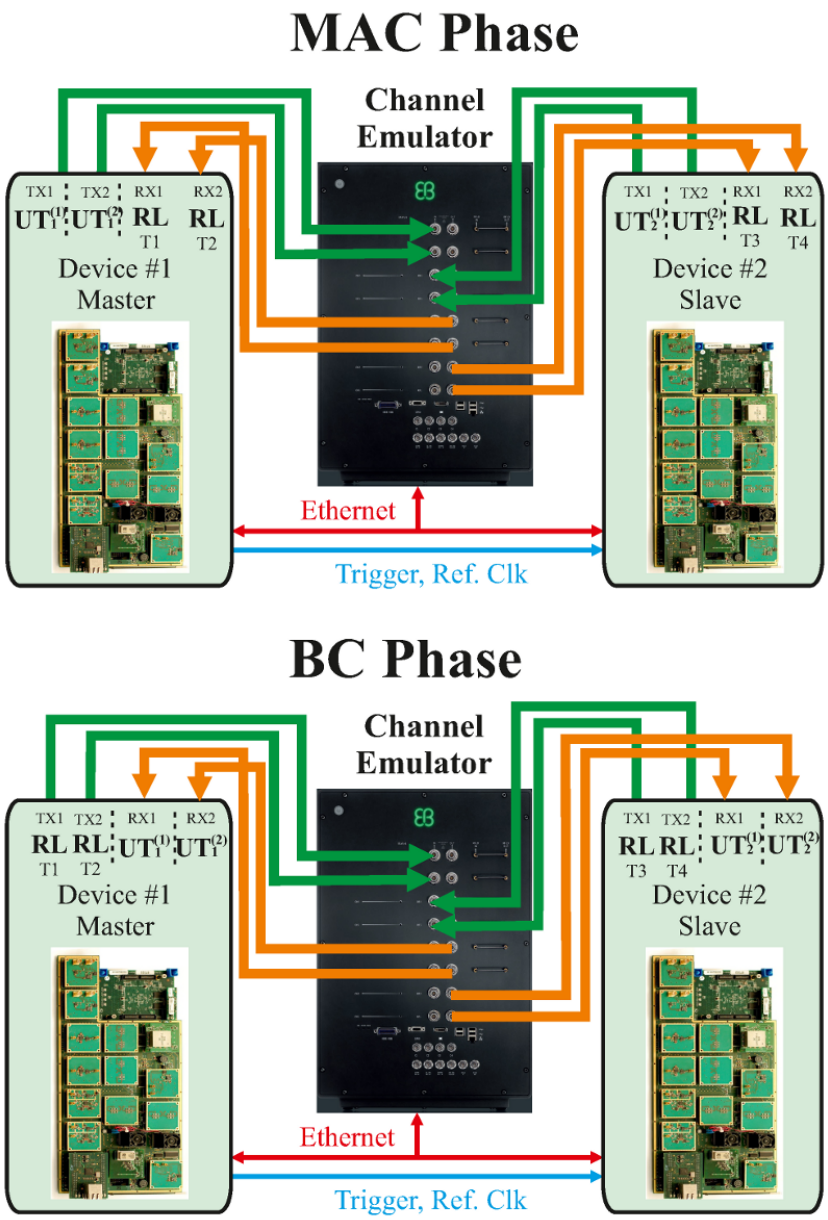

Figure 6.65: Mapping of scenario SC1-TC-II on the HIL platform with channel emulator mode. The MAC phase and the BC phase have different mappings to allow reuse of the available Tx- and Rx antennas.

realization, different SNR levels are applied by adjusting the variable gain amplifiers at the modulators. For each channel realization and each SNR level, signal transmissions in the MAC and the BC phases with both non-spectrum sharing and spectrum sharing are carried out one after another. In the sharing case, different relay algorithms are applied. During each transmission, some intermediate results e.g. the received signal constellation and the currently measured throughput can be shown. After all transmissions are finished, the results will be evaluated and saved.

6.4.5 HIL-Measurement Results

In the HIL test, OFDM signals with 512 subcarriers and CP length of 32 samples were transmitted. In the non-sharing case, each operator transmits in half of the available spectrum using a BD ANOMAX scheme. The transmission bandwidth was about 125 MHz. Rayleigh channels with 16 taps were used. The following different enabling algorithms for spectrum sharing were applied and compared: BD ANOMAX, BD RRANOMAXwf ("wf" means water filling), RBD ANOMAX, RBD RRANOMAXwf, ZF and MMSE. The carrier frequency of 2.4 GHz. For all the proposed schemes, we use a per-subcarrier power constraint. Different SNRs at the relay as well as at the UTs are achieved by adjusting the Tx power. Fig. 6.67 shows the estimated channel frequency response of the Rayleigh channels including the influence of the RF chains. Fig. 6.68 shows the measured received signal QPSK constellation of a subset of the applied algorithms (the SNR was about 25 dB). Both cases with and without spectrum sharing are shown. As shown, the interference and noise levels of the received signals of the proposed schemes in the spectrum sharing case are similar to the case without spectrum sharing. However, the interference and noise level of the MMSE scheme is considerably higher (This actually also happens to the ZF scheme).

Fig. 6.69 shows the measured sum rates (capacity) of the different relay signal processing schemes for spectrum sharing as well as of the non-sharing case as functions of SNR. Fig. 6.70 shows the corresponding CCDF of the measured sum rate (capacity) at the SNR of about 28 dB for reference. Furthermore, Fig. 6.71 and Fig. 6.72 show the corresponding per user sum rate and CCDF, respectively. As shown in Fig. 6.69, when the SNR is sufficiently high (e.g. higher than 22 dB), spectrum sharing gain can be achieved. Furthermore, the higher the SNR, the larger the spectrum sharing gain. We can also see that if the SNR is only medium or low (e.g. lower than 22 dB) and an improper scheme is applied, the sum rate can even be lower than that without spectrum sharing. In this case, the ZF scheme is such improper scheme. Generally, the proposed schemes outperform the ZF and MMSE (which are state-of-the-art), except for the low SNR region. The higher the SNR, the more advantage the proposed schemes have. Among the proposed schemes, RBD ANOMAXwf shows the best performance. However, the performance difference between the proposed schemes is relatively small. Therefore, when choosing such schemes, we should also consider the aspects of computational complexity and

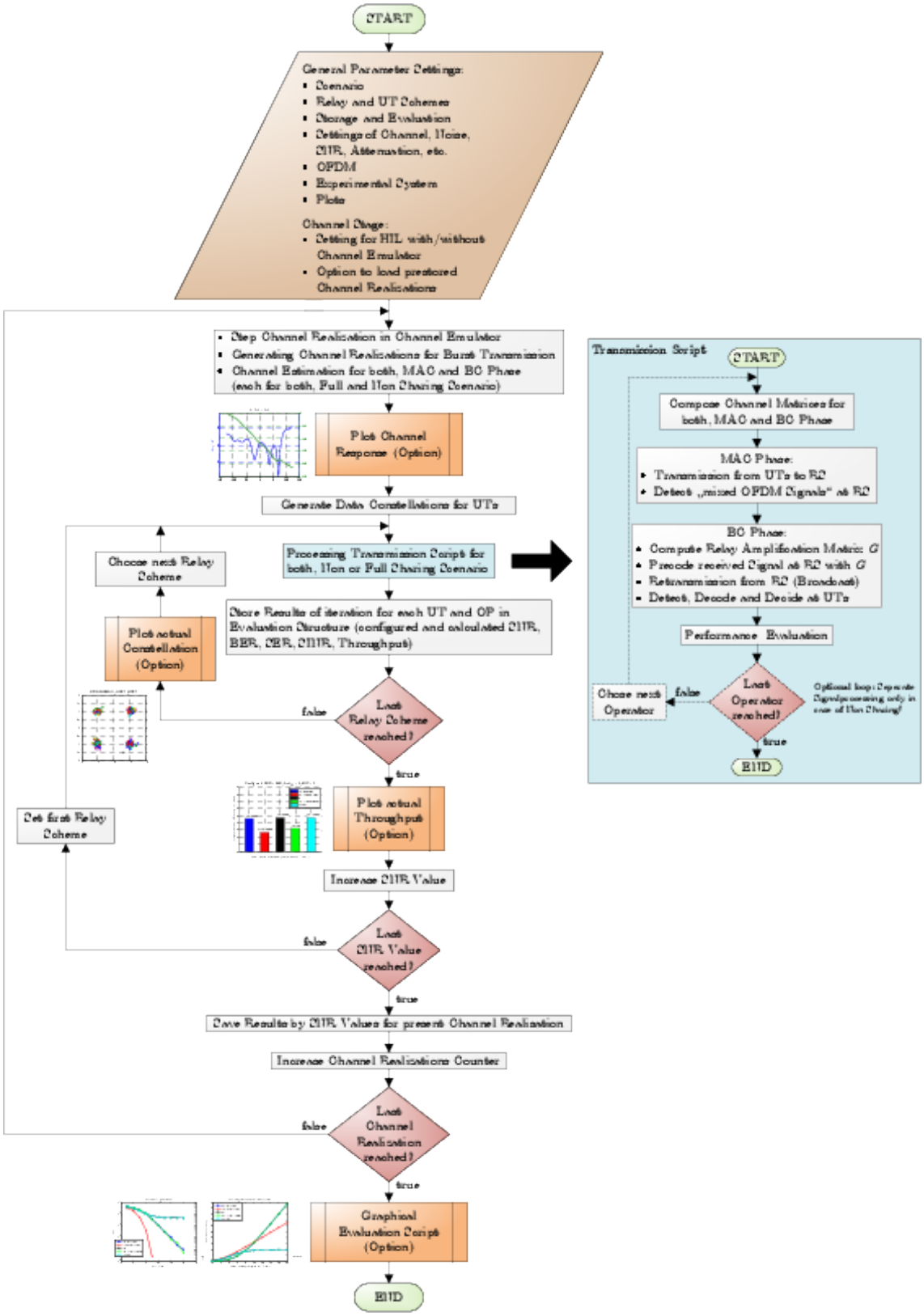

Figure 6.66: Flowchart of the software implementation of the TWR scenario.

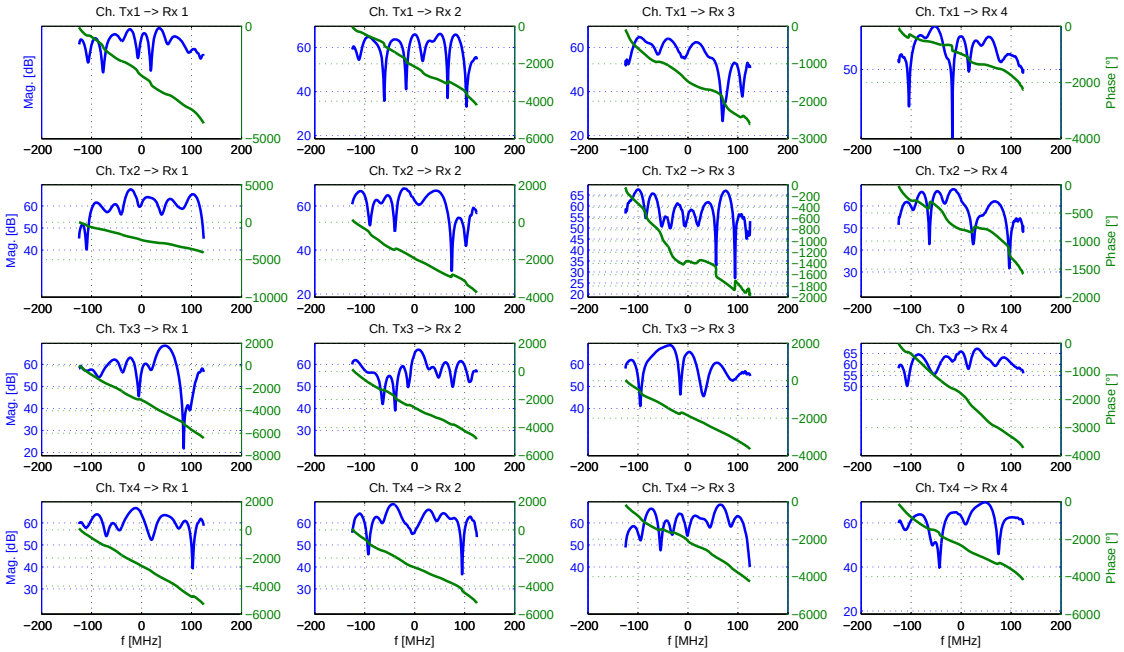

Figure 6.67: Estimated frequency response of the Rayleigh channels in the channel emulator for the TWR scenario.

communication overhead. One example is that BD does not need power noise information at the relay and thus, has lower communication overhead (no need to feed back the noise power information to the relay) than RBD.

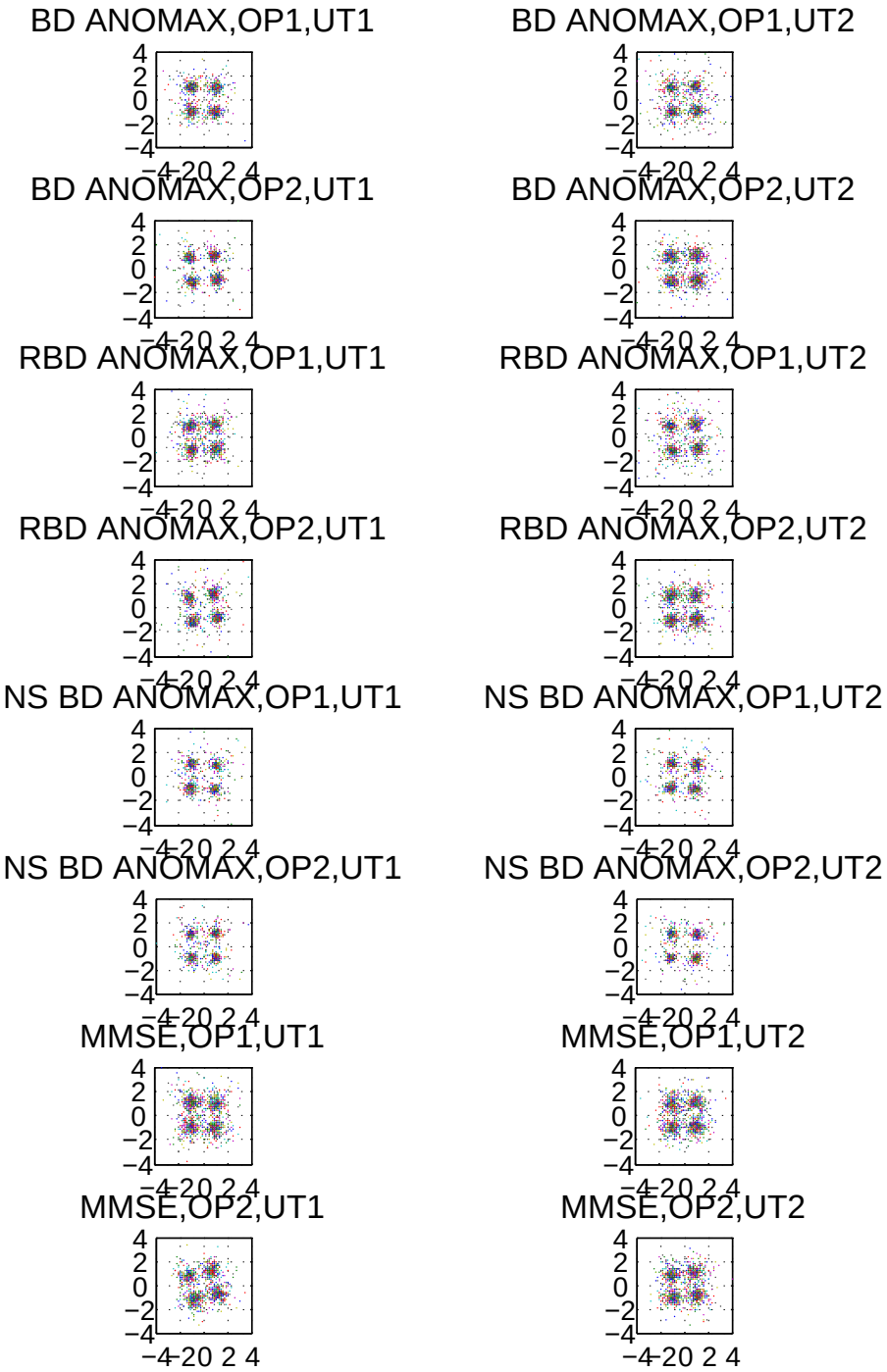

Figure 6.68: Measured received signal QPSK constellation of a subset of the applied algorithms. Both cases with and without spectrum sharing are shown. Due to restriction of space, not all the applied algorithms are given.

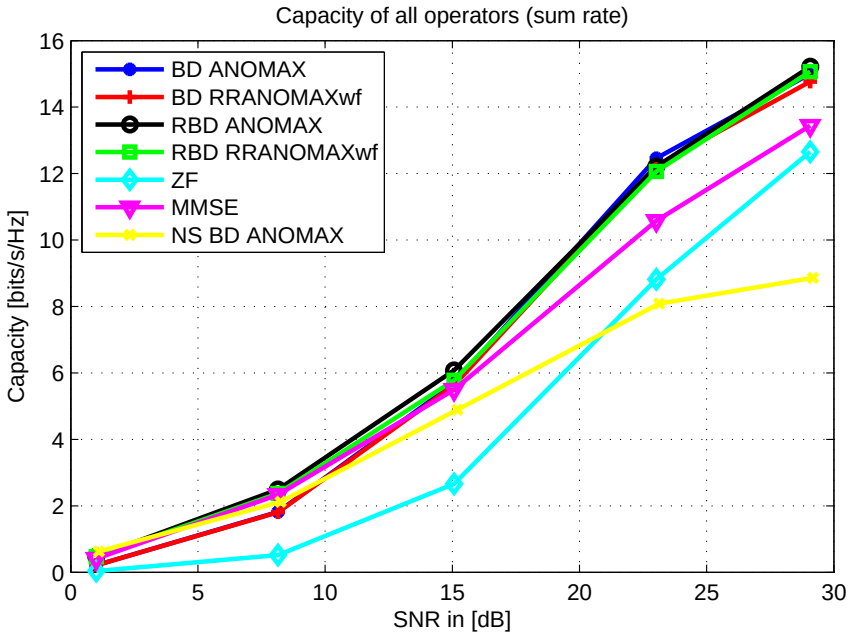

Figure 6.69: Measured sum rate vs. SNR in the TWR scenario.

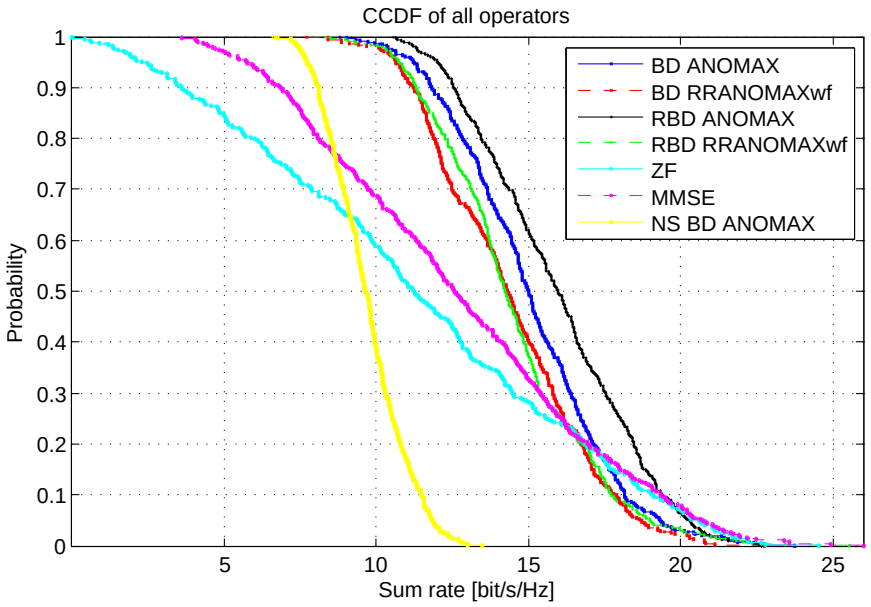

Figure 6.70: CCDF of the measured sum rate at the SNR of about 28 dB.

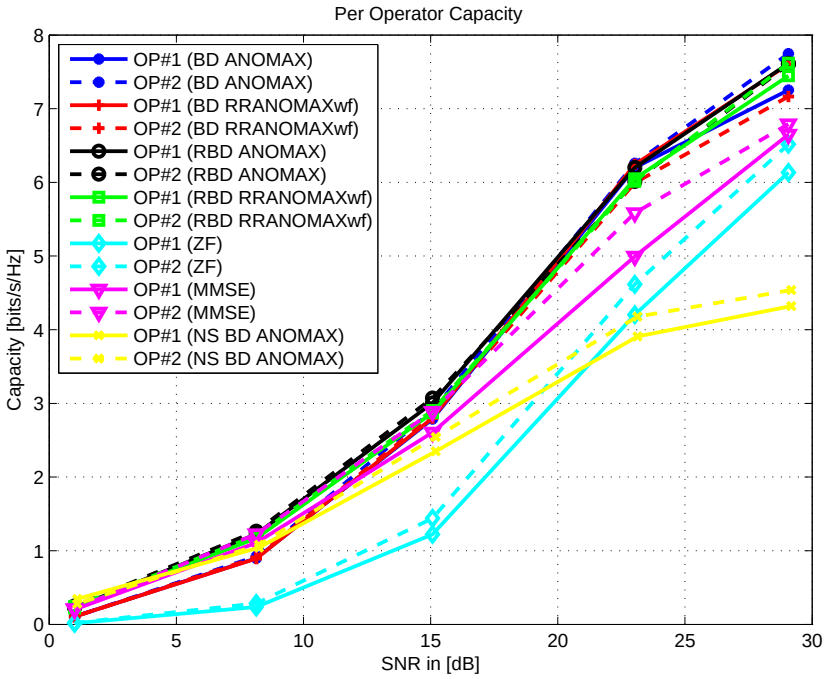

Figure 6.71: Measured per-operator rate vs. SNR in the TWR scenario.

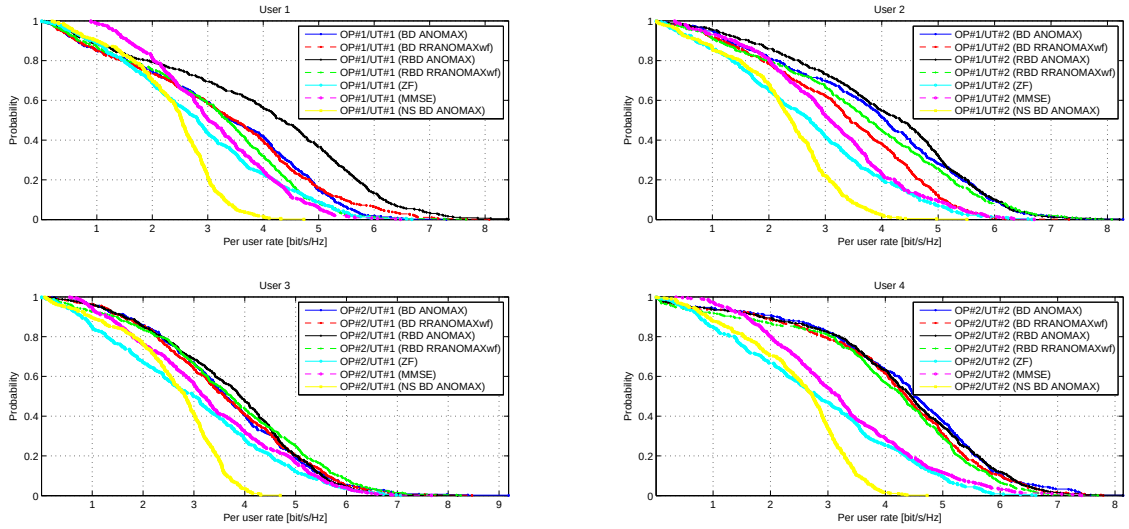

Figure 6.72: CCDF of the measured per-operator rate at the SNR of about 28 dB.

7 Implementation and Evaluation on the LTE-Advanced Testbed

7.1 Scenario SC2-TA: Spectrum Sharing

7.1.1 Scenario and Test Case Description

This scenario was already described in Sec. 6.1.1. As discussed both internally within SAPHYRE and with EAB members, this scenario is most representative and is most close to the current industry trend. Therefore, this scenario is selected for the real-time implementation on the LTE-Advanced testbed. However, unlike on the HIL demonstrator platform, we have chosen different test cases for the implementation on the LTE-Advanced testbed.

The test case for spectrum sharing in LTE-Advanced is the dynamical coordination of common spectrum access among mobile operators. To be more concrete, two mobile operators share an amount of spectrum, which can consists of subsets of the licensed spectra of both operators or can be owned by a third party. In our implementation and demonstration, we consider the case that the shared spectrum consists of two halves, each originally owned by one operator. Fig. 7.1 illustrates this test case. On this shared spectrum, only orthogonal sharing is allowed i.e. in each frequency resource unit, only one operator can transmit signals. Each mobile operator can in principle allocated any frequency resource units from this shared spectrum, as long as this is in agreement with the other operator. Therefore, such frequency resource allocation should be done in a coordinated way among both mobile operators. The coordination of the frequency resource allocation should follow a set of predefined rules which both mobile operators have agreed on. Such coordinated frequency resource allocation requires the dynamic exchange of information between the network operators, such as the instantaneous traffic served in each network and channel quality indicators (CQI) for terminals with high traffic demands. Despite common spectrum access, the shared spectrum is still used in an orthogonal way in this test case.

It is potentially possible to extend this test case to non-orthogonal spectrum sharing. By introducing advanced multi-antenna techniques, spatial reuse of the radio resources is made possible. By exchange of channel state information (CSI) inside and between the networks, inter-cell interference cancellation is enabled. If user data are exchanged in addition, joint transmission coordinated multipoint (JT-CoMP) can be used.

Since operators often use hardware from different vendors, the interfaces for the required information exchange need to be standardized and, as mentioned above, common rules for sharing the limited amount of radio resources have to be agreed on.

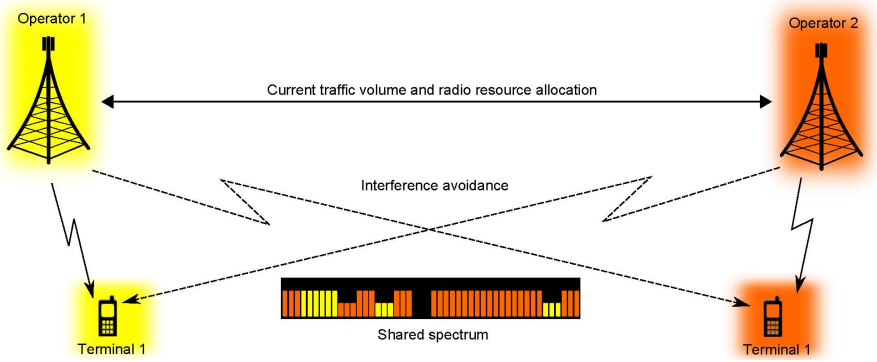

Figure 7.1: Spectrum sharing scenario on the LTE-Advanced testbed.

7.1.2 Mapping and Implementation on the LTE-Advanced Platform

The goal of the implementation on the LTE-Advanced platform is to demonstrate that spectrum sharing can be realized in realtime in a distributed manner, in other words, without any centralized control unit. This is an essential requirement for the feasibility of the approach in the distributed LTE network architecture.

The mapping of the spectrum sharing scenario on the LTE-Advanced testbed is illustrated in Fig. 7.2, where the two LTE BS devices below play the roles of the BS's of both operators. The two LTE UT devices play the roles of the UT's of both operators. Unlike the BS devices, each UT device can play the role of multiple UT's of an operator, which are illustrated in the screen in Fig. 7.2. In the demonstration, the different UT's of an operator are indicated by separate transmissions of video streams. Furthermore, each BS/UT device can both transmit and receive, i.e. both LTE downlink and uplink are demonstrated. For the downlink, operator 1 and Operator 2 have 10 MHz bandwidths each at the center frequencies 2.55 GHz and 2.65 GHz. Moreover, the downlink transmission is carried out over a 2×2 MIMO configuration with adaptive modulation (from BPSK upto 64-QAM). In the uplink, the carrier frequencies of operator 1 and 2 are 2.525 GHz and 2.535 GHz, respectively. Also, the transmission bandwidth of each operator is 10 MHz. Moreover, only SISO transmission is possible, with a fixed modulation of QPSK. With the LTE-Advanced testbed, free space wave propagation at 2.6 GHz carrier frequency is possible, if a license is available. If the license is not available, a "channel in the box" device is used to emulate the radio channel. First, all Tx- and Rx antennas are placed into a metal box, which isolates the transmitted RF signals. Second, a device consisting of rotating metal object is placed into this box to generate time variation

of this emulated radio channel. With such a mapping, the effect of time variant radio channels can be included, which affect the CSI feedback and the resource allocation.

To achieve frequency and time synchronization between both BS's, a Rubidium-Normal module is used to generate an accurate 38.4 MHz baseband clock, an accurate 10 MHz reference clock and a 1-pps pulse. For the synchronization of the sampling frequency, the 38.4 MHz baseband clock is distributed via cables to both BS's. For 10 MHz reference clock is for an LO to generate an LO signal of 2.6 GHz, which is distributed to the RF-frontends of the BS's via cables. Afterwards, the modulations to the 2.55 GHz and 2.65 GHz carrier frequencies by both BS's are done with digital IF up conversion. For time synchronization, the 1-pps pulse signal is distributed to both BS's via cables.

7.1.3 Enabling Algorithm

For simultaneous access to the compound spectrum by both operators, information is exchanged and common rules are defined. As mentioned above, operator 1 and Operator 2 have 10 MHz bandwidths each at the center frequencies 2.55 and 2.65 GHz. Eight frequency sub-bands can be assigned within each part of the spectrum. The UTs' measure the current traffic volume and the feasible data rate and feed it back over the up-link together with the current resource map. The reason for this is that measuring this information at the UT's was easier from an implementation point of view as normally this information is already given at the serving base station.

Afterwards, the operators exchange this information over the network interconnect. Each BS calculates the capacity consumed in each network from both resource maps and knows which resources can be assigned additionally in their own and in the other operator parts of the spectrum. In a following stage, the resources are assigned individually by each network following a common set of rules. This is done by switching data streams on or off using a linear pre-coder at the transmitter side.

For the dynamic frequency resource allocation among both operators, the following common rules are deployed and implemented in the realtime in the LTE-Advanced demonstrator:

1. Each operator starts by using its own resources first, as long as traffic is smaller than the capacity limit;
2. Unused resources in the compound spectrum are assigned by a fixed rule only if an operator's own resources are completely consumed;
3. If additional resources are no longer used, the worst resource is always released, i.e. sharing is opportunistic and channel-aware;
4. Resources are given back to the spectrum owners if they require additional

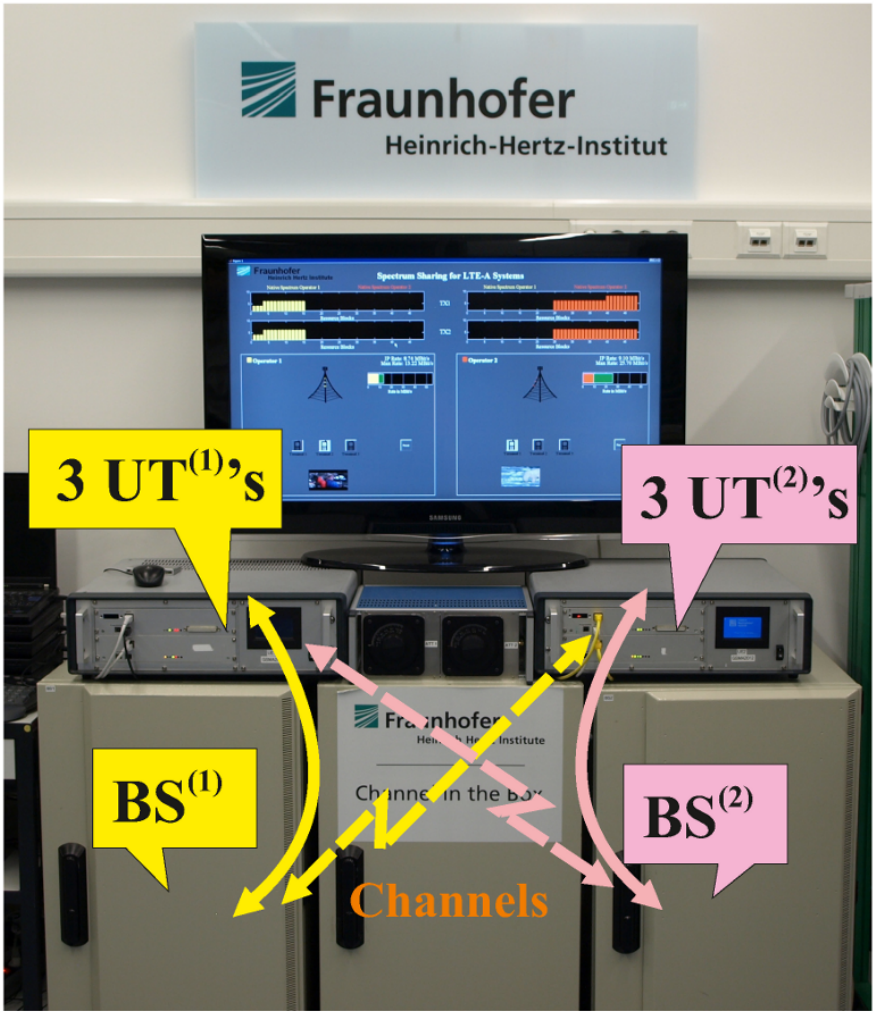

Figure 7.2: Mapping of the spectrum sharing scenario on the LTE-Advanced testbed.

spectrum room, but there are no more free resources available in the compound spectrum;

5. If the load is simultaneously high in both networks, operators move back to their own parts of the spectrum. The last two rules are needless in LTE Rel. 11/12 if CSI is available at base stations and inter-cell interference cancellation techniques can be used.

7.1.4 Live Demonstration of Spectrum Sharing on the LTE-Advanced Testbed

7.1.4.1 Illustration of the Live Demonstration

After realtime implementation, the spectrum sharing scenario can be demonstrated in live. Fig. 7.3 shows a screenshot of the live demonstration. As we can see, the allocated frequency resources for the two operators are shown on the left- and the right hand side of this figure. The allocated amount of frequency resources scales with the data load, which can be seen from the number of active UTs (indicated by the different video streams) of each operator (lower part of the figure). By using the frequency resource of operator 2, the data throughput of operator 1 can be enhanced to cope with the high load.

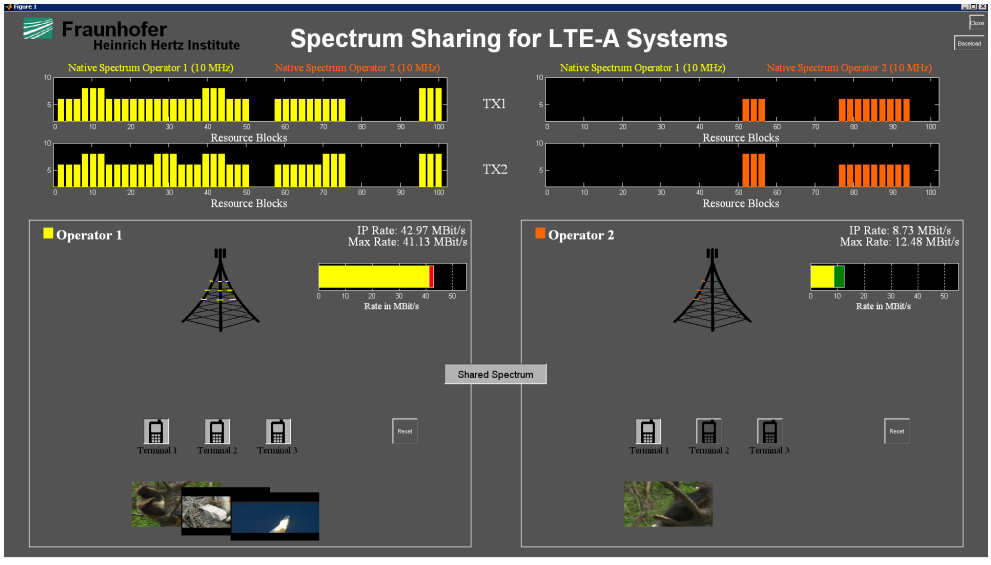

Figure 7.3: Screenshot of the initial LTE-Advanced demonstration on spectrum sharing.

7.1.4.2 Demonstration on Mobile World Congress 2012 and Future Network and Mobile Summit 2012

The implemented spectrum sharing demonstration on the LTE-Advanced testbed has been successfully demonstrated on the important events Mobile World Congress (MWC) 2012 in Barcelona, Spain, and Future Network and Mobile Summit (FNMS) 2012, Berlin, Germany. Fig. 7.4∼ Fig. 7.5 show the demonstrator setup and the demonstration activities on MWC 2012, while Fig. 7.6∼ Fig. 7.7 show those on FNMS 2012. On both events, the LTE-Advanced spectrum sharing demonstration has received a lot of positive feedbacks and comments. A lot of discussions were about the enabling infra-structure for spectrum sharing, especially regarding the backhaul for inter-operator information exchange, so that the spectrum allocation can be done in a coordinated but distributed way. With the live LTE-Advance demonstration, the visibility of the SAPHYRE project is significantly enhanced. Since a lot of industry interest on spectrum sharing has been invoked due to the demonstrations on these important events, a significant step of SAPHYRE has been made towards the industry.

Figure 7.4: LTE-Advanced spectrum sharing demonstration setup on Mobile World Congress (MWC) 2012.

Figure 7.5: LTE-Advanced spectrum sharing demonstration on Mobile World Congress (MWC) 2012.

Figure 7.6: LTE-Advanced spectrum sharing demonstration setup on Future Network and Mobile Summit (FNMS) 2012.

Figure 7.7: LTE-Advanced spectrum sharing demonstration on Future Network and Mobile Summit (FNMS) 2012.

8 Summary and Conclusions

In this deliverable, the scenario and test case implementation and evaluation on two demonstrator platforms are reported. The two demonstrator platforms are: 1) The flexible HIL platform; 2) The LTE-Advanced testbed. First, an overview of the selected scenarios and test cases for implementation is given. Afterwards, the scenario implementation work flow is described, which includes the interaction between WP6 and the other WPs. The important functionalities of the HIL-demonstrator platform as well as the LTE-Advanced testbed are described.

For HIL-demonstrator platform, the test case implementation and evaluation of four scenarios are reported. 1) The first one is the spectrum sharing scenario without base-station collocation. In this scenario, advanced transmit beam-forming techniques were applied to enable spectrum sharing gains, which is evaluated by the achievable sum rate. HIL test results show that by sharing the spectrum via a proper algorithm, considerable sum rate gain can be achieved. Furthermore, we found out that the weaker the interference links, the higher the spectrum sharing gain. We further observed that the proposed beam-forming techniques work well under low mobility of the UT's. However, with high UT mobility, strong performance degradation can be observed. Therefore, improved techniques or alternative techniques should be developed for the high mobility cases. Finally, among the proposed algorithms, a tradeoff between performance, complexity and communication overhead exists. 2) The second one is the full sharing (spectrum and base-station) scenario. In this scenario, advanced precoding techniques were applied to enable spectrum sharing assuming shared BS hardware. HIL test results show that considerable sum rate gain can be achieved by sharing the spectrum. Similar to the first scenario, for the proposed algorithms, a tradeoff exists between performance, complexity and communication overhead. 3) The third scenario is a relay sharing scenario in a "butterfly" network, where advanced network coding techniques were applied to enable spectrum sharing in such a network. HIL test results show that in the practical SNR regions of the direct links and the C-SI links, considerable capacity gain can be achieved by spectrum sharing. Furthermore, the proposed Hierarchical Decode and Forward (HDF) technique outperforms the state-of-the-art Amplify-and-Forward with Successive Interference Cancellation (SIC) technique. 4) The fourth scenarios is also a relay sharing scenario but in a Two-Way-Relaying (TWR) network. In this scenario, advanced multi-antenna signal processing techniques were applied at the relay to allow spectrum sharing gain. HIL test results show that with proper relay signal processing techniques, considerable sum rate gain can be achieved by spectrum sharing. Furthermore, the proposed techniques considerably outperform the state-of-the-art techniques. For all four scenario above,

the practical implementation problems are identified. To solve some of these problems, the proposed enabling algorithms have been improved and optimized. To cope with other problems, practical concepts and solutions are described and discussed. The HIL-demonstration of these four scenarios have been successfully shown in SAPHYRE project workshops.

For the LTE-Advanced testbed, the spectrum sharing scenario is selected for real-time implemention and live demonstration. The corresponding experimental setup, test case definition and implementation were described. This implementation shows the orthogonal spectrum sharing case and includes the advanced functionalities e.g. CSI feedback via uplink, adaptive modulation and advanced resource allocation. This live demonstration dynamically allocating the shared spectrum to different operators, considerable throughput gain and user experience enhancement can be observed. This demonstration has been successfully shown on the important events Mobile World Congress (MWC) 2012 and Future Network and Mobile Summit (FNMS) 2012. On both events, a lot of industry interests on spectrum sharing have been invoked. Thus, a significant step of SAPHYRE has been made towards the industry.

Based on the implementation and demonstration results on both demonstrator platforms, we can see that resource sharing is feasible in wirless networks and can achieve considerable gains. For the exploitation of resource sharing, sophisticated and carefully designed algorithms are necessary, which takes the practical implementation problems into account.

Bibliography

[1] E. A. Jorswieck, L. Badia, T. Fahldieck, D. Gesbert, S. Gustafsson, M. Haardt, K.-M. Ho, E. Karipidis, A. Kortke, E. G. Larsson, H. Mark, M. Nawrocki, R. Piesiewicz, F. R¨omer, M. Schubert, J. Sykora, P. Trommelen, B. van den Ende, and M. Zorzi, "Resource sharing in wireless networks: The SAPHYRE approach," in *Proc. of Future Network and Mobile Summit (FNMS'10)*, Jun. 2010, pp. 1–8.

[2] E. A. Jorswieck, "Framework for beamforming in interference networks: Multicast, MISO IFC and secrecy capacity," in *International Zürich Seminar on Communications*, 2010.

[3] J. Lindblom and E. Karipidis, "Cooperative beamforming for the MISO interference channel," in *Proc. of IEEE European Wireless Conference (EW'10)*, Lucca, Italy, 2010.

[4] F. Römer, J. Zhang, M. Haardt, and E. Jorswieck, "Spectrum and infrastructure sharing in wireless networks: A case study with relay-assisted communications," in *Proc. of Future Network and Mobile Summit (FNMS'10)*, Jun. 2010.

[5] Z. K. M. Ho, M. Kaynia, and D. Gesbert, "Distributed power control and beamforming on MIMO interference channels," in *Proc. of IEEE European Wireless Conference (EW'10)*, Apr. 2010, pp. 654–660.

[6] J. Sykora and A. Burr, "Network coded modulation with partial side-information and hierarchical decode and forward relay sharing in multi-source wireless network," in *Proc. of IEEE European Wireless Conference (EW)'10*, Apr. 2010, pp. 1–7.

[7] J. Li, F. Römer, and M. Haardt, "Linear precoding design in MIMO interference relay channels," in *Proc. of IEEE International Conference on Acoustics, Speech and Signal Processing (ICASSP'11)*, May 2011.

[8] R. Mochaourab and E. A. Jorswieck, "Exchange economy in two-user multiple-input single-output interference channels," *IEEE J. Sel. Topics Signal Process.*, 2011, accepted for publication.

[9] ——, "Optimal beamforming in interference networks with perfect local channel information," *IEEE Trans. Signal Process.*, Mar. 2011.

[10] ——, "Walrasian equilibrium in two-user multiple-input single-output interference channel," in *Proc. IEEE International Conference on Communications*

(ICC'11), Kyoto, Japan, 2011.

[11] M. Haardt, Z. K. M. Ho, E. Jorswieck, and et al., "Saphyre project deliverable d3.1b: Adaptive and robust signal processing in multi-user and multi-cellular environments (final)," 2012.

[12] J. Sykora, M. Hekrdla, P. Prochazka, and T. Uricar, "Network, resource, and interference aware coding and decoding (final)," 2012.

[13] T. Fahldieck and H. Z. et al., "Resource allocation and interference management strategies," 2011.

[14] M. Stege, F. Schafer, M. Henker, and G. Fettweis, "Hardware in a loop-a system prototyping platform for MIMO-approaches," in *ITG Workshop on Smart Antennas*, Mar. 2004, pp. 216–222.

[15] L. Zu, P. Wang, J. Han, F. Liu, Q. Ai, and Y. Ji, "A study on test platform for verifying new wireless networking technologies via hardware-in-loop simulation," in *Proc. of International Conference on Cyber-Enabled Distributed Computing and Knowledge Discovery (CyberC'10)*, Oct. 2010, pp. 75–78.

[16] G. Fettweis, M. Löhning, D. Petrovič, M. Windisch, P. Zillmann, and W. Rave, "Dirty RF: a new paradigm," in *Proc. of IEEE International Symposium on Personal, Indoor and Mobile Radio Communications (PIMRC'05)*, vol. 4, Sep. 2005, pp. 2347–2355.

[17] J. Luo and A. Kortke, "SAPHYRE project deliverable D6.2: Internal report on demonstrator platform development," Fraunhofer Gesellschaft (FhG), Heinrich-Hertz-Institut (HHI), Tech. Rep., 2010.

[18] J. Luo, A. Kortke, W. Keusgen, J. Li, M. Haardt, P. Prochazka, and J. Sykora, "A flexible hardware-in-the-loop test platform for physical resource sharing mechanisms in wireless networks," in *Proc. of Future Network and Mobile Summit (FNMS'11)*, Jun. 2011.

[19] J. Luo, J. Lindblom, J. Li, R. Mochaourab, A. Kortke, E. Karipidis, M. Haardt, E. Jorswieck, and E. G. Larsson, "Transmit beamforming for inter-operator spectrum sharing: From theory to practice," in *Proc. International Symposium on Wireless Communication Systems (ISWCS'12)*, 2012, submitted.

[20] D. Gesbert, J. Kibilda, and M. H. et al., "Saphyre reference scenario parameters and novel interference models (final)," 2011.

[21] T. Janssen, A. Pais, and H. Z. et al., "Reference scenarios for resource sharing (final)," 2011.

[22] J. Luo, A. Kortke, J. Li, P. Prochazka, and J. Sykora, "Saphyre project deliverable d6.1b: Scenario definition and test case selection for demonstrator platform evaluation (final)," 2010.

[23] V. Jungnickel and et al., "Field trials using coordinated multi-point transmis-

sion in the downlink," in *Proc. IEEE International Symposium on Personal, Indoor and Mobile Radio Communications (PIMRC'10) Workshops*, sept. 2010.

[24] Q. H. Spencer, A. L. Swindleherst, and M. Haardt, "Zero-forcing methods for downlink spatial multiplexing in multiuser MIMO channels," *IEEE Trans. Signal Process.*, Feb. 2004.

[25] V. Stankovic and M. Haardt, "Generalized design of multi-user MIMO precoding matrices," *IEEE Trans. on Wireless Commun.*, vol. 7, Mar. 2008.

[26] E. A. Jorswieck, E. G. Larsson, and D. Danev, "Complete characterization of the Pareto boundary for the MISO interference channel," *IEEE Trans. Signal Process.*, vol. 56, no. 10, Oct. 2008.

[27] R. Mochaourab, E. A. Jorswieck, K. M. Z. Ho, and D. Gesbert, "Bargaining and beamforming in interference channels," in *Proc. Annual Conference on Signals, Systems, and Computers (Asilomar'10)*, Nov. 2010.

[28] G. A. Jehle and P. J. Reny, *Advanced Microeconomic Theory*, 2nd ed., ser. Addison-Wesley. Pearson Education, 2003.

[29] E. G. Larsson and E. A. Jorswieck, "Competition versus cooperation on the MISO interference channel," *IEEE Journal on Selected Areas in Comm.*, Sep. 2008.

[30] P. Popovski and H. Yomo, "Physical network coding in two-way wireless relay channels," in *Proc. of IEEE International Conference on Communications (ICC'07)*, Jun. 2007, pp. 707–712.

[31] V. Jungnickel, T. Wirth, M. Schellmann, T. Haustein, and W. Zirwas, "Synchronization of cooperative base stations," in *IEEE International Symposium on Wireless Communication Systems (ISWCS '08)*, 2008.

[32] F. Roemer, E. Jorswieck, and M. Haardt, "Efficient spatial processing and resource allocation for amplify and forward two-way relaying," *Cross Layer Designs in WLAN Systems, N. Zorba and C. Skianis and C. Verikoukis, eds., Troubador Publishing Ltd, Leicester, UK*, 2010.

[33] T. Unger and A. Klein, "Duplex schemes in multiple antenna two-hop relaying," *EURASIP Journal on Advances in Signal Processing*, 2008.

[34] J. Joung and A. H. Sayed, "Multiuser two-way amplify-and-forward relay processing and power control methods for beamforming systems," *IEEE Trans. Signal Process.*, vol. 58, pp. 1833–1846, Mar. 2010.